https://doi.org/10.5194/egusphere-2022-401
Preprint. Discussion started: 13 June 2022

Climate response to off-equatorial stratospheric sulfur injections in three Earth System Models - Part 1: experimental protocols and surface changes

Daniele Visioni[1], Ewa M. Bednarz[1], Walker R. Lee[1], Ben Kravitz[2,3], Andy Jones[4], Jim M. Haywood[4,5], and Douglas G. MacMartin[1]

[1]Sibley School of Mechanical and Aerospace Engineering, Cornell University, Ithaca, NY, USA
[2]Department of Earth and Atmospheric Science, Indiana University, Bloomington, IN, USA
[3]Atmospheric Sciences and Global Change Division, Pacific Northwest National Laboratory, Richland, WA, USA
[4]Met Office Hadley Centre, Exeter, UK
[5]College of Engineering, Mathematics and Physical Sciences, University of Exeter, Exeter, UK

Correspondence: Daniele Visioni (dv224@cornell.edu)

Abstract. There is now a substantial literature of climate model studies of equatorial or tropical stratospheric SO_2 injections that aim to counteract the surface warming produced by rising concentrations of greenhouse gases. Here we present the results from the first systematic intercomparison of climate responses in three Earth System Models where the injection of SO_2 occours at different latitudes in the lower stratosphere. Our aim is to determine commonalities and differences between the climate model responses in terms of the distribution of the optically reflective sulfate aerosols produced from the oxidation of SO_2, and in terms of the surface response to the resulting reduction in solar radiation. A focus on understanding the contribution of characteristics of models transport alongside their microphysical and chemical schemes, and on evaluating the resulting stratospheric responses in different models is given in the companion paper (Bednarz et al., 2022). The goal of this exercise is not to evaluate these single point injection simulations as stand-alone proposed strategies to counteract global warming; instead we determine sources and areas of agreement and uncertainty in the simulated responses and, ultimately, the possibility of designing a comprehensive intervention strategy capable of managing multiple simultaneous climate goals through the combination of different injection locations. We find large disagreements between GISS-E2.1-G and the CESM2-WACCM6 and UKESM1.0 models regarding the magnitude of cooling per unit of aerosol optical depth (AOD) produced, from 4.7 K per unit of AOD in CESM2-WACCM6 to 16.7 K in the GISS-E2.1-G version with modal aerosol microphysics. By normalizing the results with the global mean response in each of the models, and thus assuming that the amount of SO_2 injected is a free parameter that can be managed independently, we highlight some commonalities in the overall distributions of the aerosols, in the inter-hemispheric surface temperature response and in shifts to the Inter-Tropical Convergence Zone, and also some areas of disagreement, such as the aerosol confinement in the equatorial region and the transport to polar latitudes.

https://doi.org/10.5194/egusphere-2022-401
Preprint. Discussion started: 13 June 2022

1 Introduction

A climate model is an imperfect representation of the real climate system, having to deal with simplified processes across spatial and temporal scales, bound both by technical limits to the computational capabilities and by fundamental uncertainties in some of the underlying processes. Reducing such uncertainties can be a complicated process and may leverage various strategies: by simulating current and past climates for which we have available observations, the skills of current climate models can be evaluated and the reliability of future projections assessed (Brunner et al., 2020). The use of large ensembles of simulations can further help to narrow down some of the uncertainties by isolating biases due to internal model variability over time (Deser et al., 2012; Lehner et al., 2020). Finally, the use of multiple climate models can help to clarify some of the sources of uncertainty by analyzing the response to an external forcing in multiple independent models. This has been done in numerous generations of the Climate Model Intercomparison Project (CMIP) (Masson and Knutti, 2011; Boucher et al., 2013; Tebaldi et al., 2021), which addresses the effects of an increased CO_2 forcing on the global and regional surface climate (Hawkins and Sutton, 2011). Other modeling exercises such as the Chemistry-Climate Model Initiative (Morgenstern et al., 2018) have used models with explicit atmospheric chemistry coupling (which many of the CMIP models lack) to determine the future evolution of key atmospheric variables, such as stratospheric ozone (Dhomse et al., 2018) and stratospheric circulation (Eichinger et al., 2019). Finally, model intercomparisons have been designed to constrain the response of climate models to explosive volcanic eruptions, trying to understand both the evolution of the aerosol cloud over time (Timmreck et al., 2018) and its climatic effects (Clyne et al., 2021).

The assessment of simulated climate intervention techniques presents all of the challenges discussed above, but also novel ones. The proposed injection of sulfur dioxide (SO_2) to temporarily cool the planet (stratospheric aerosol intervention, SAI) while greenhouse gas levels are reduced (Crutzen, 2006) has been studied with climate models in the last two decades, and multiple intercomparisons have been carried out spearheaded by the Geoengineering Model Intercomparison Project (GeoMIP, Kravitz et al. (2011)). The first SAI experiments, GeoMIP G3 and G4 (Kravitz et al., 2011), prescribed the injection of SO_2 in the equatorial stratosphere (in a time-varying or constant manner, respectively). However, the modeling teams were free to specify the exact details of the injection "in the same manner as they simulate a volcanic eruption"; this led to differences in the approaches chosen. For instance, ULAQ-CCM injected SO_2 between 18 and 25 km of altitude using a Gaussian distribution, whereas GEOSCCM injected SO_2 uniformly between 16 and 25 km of altitude. The varying experimental protocols resulted in large differences in the simulated aerosol distributions, which compounded the differences coming from the differences in the representation of aerosol microphysics amongst the models (Visioni et al., 2017). More recently, the GeoMIP experiment G6 (Kravitz et al., 2015) prescribed variable injections of SO_2 between 10°N and 10°S, and between 18 and 20 km of altitude. However, some models lacking interactive aerosol treatment prescribed an aerosol distribution from sources not entirely consistent with the original prescription for models without interactive microphysics, resulting in challenges in the attribution of the causes of some of the resulting discrepancies (Visioni et al., 2021). Lastly, the test-bed experiment described by Weisenstein et al. (2021) prescribed two injection scenarios (one uniformly between 18 and 20 km, and between

https://doi.org/10.5194/egusphere-2022-401
Preprint. Discussion started: 13 June 2022

30°N and 30°S; and one in two precise locations, 30°N and 30°S, at 19 km of altitude) to understand inter-model differences between injections of SO_2 and direct injections of accumulation mode H_2SO_4 to better control the size of the resulting aerosols.

In parallel, simulations with the Community Earth System Model version 1 with the Whole Atmosphere Community Climate Model (CESM1(WACCM)) were carried out examining how changes in the location of the sulfate injection matters for the climatic impacts. Tilmes et al. (2017) injected SO_2 at 4 locations (30°N, 15°N, 15°S and 30°S) and showed that they resulted in different aerosol distributions and in different atmospheric and surface responses (see also Richter et al. (2017); Tilmes et al. (2018b)). Further, MacMartin et al. (2017) showed that these SO_2 injection locations could be combined to achieve multiple climate goals with the use of a feedback algorithm capable of deciding each year how much SO_2 to inject at each of the aforementioned latitudes (Kravitz et al., 2017). The four locations of injection were necessary to control the overall geographical distribution of the simulated aerosols and, thus, to constrain not only the global mean surface temperatures, but also to make sure that the large-scale inter-hemispheric surface temperature gradient and the equator-to-pole surface temperature gradient are maintained. This approach was adopted in the Geoengineering Large Ensemble experiment (GLENS, Tilmes et al. (2018a)) that studied the feasibility and climate impacts of a potential SAI deployment strategy. By differentiating the injection locations, numerous side-effects and adverse impacts of SAI could be reduced compared to an equatorial injection strategy (Kravitz et al., 2019). Up to now, all of the above assessments, and the exploration of other strategies, have been performed with only only climate model - CESM1(WACCM).

In this work we aim to perform a first systematic intercomparison of the stratospheric and surface climate responses to the injection of SO_2 at different latitudes in the stratosphere. We use three comprehensive Earth System Models (ESMs) with interactive sulfate aerosol treatment and a set of carefully designed experiments with a single point of injection per experiment. Our goals are: i) to robustly evaluate similarities and differences in the simulated sulfate aerosol distributions and in the resulting surface and atmospheric responses; ii) to elucidate the areas and sources of intermodel differences, in particular the roles of characteristics of model microphysical schemes and biases in climatological transport; iii) to determine the reliability of estimates of the surface responses to SAI previously performed in MacMartin et al. (2017) and the middle atmospheric responses performed in Tilmes et al. (2018b); Richter et al. (2017) using the multi-model approach; and iv) to lay the ground for an intermodel comparison of SAI simulations achieving the same set of surface temperature goals using a feedback algorithm. In this paper we discuss the simulated aerosol fields and their effects on zonal mean surface temperatures and precipitation; we then use that information to determine the magnitude of SO_2 injection needed in each location to obtain the desired temperature targets. In the companion paper (Bednarz et al., 2022, hereafter PART2), the simulated differences in the aerosol distribution are explained in terms of the model differences in atmospheric circulation, and the resulting SAI impcats on stratospheric temperatures, chemistry and circulation are discussed.

https://doi.org/10.5194/egusphere-2022-401
Preprint. Discussion started: 13 June 2022

2 Earth System models used

We performed our simulations in three Earth System Models (ESMs): CESM2-WACCM6, UKESM1.0 and GISS-E2.1-G; for the latter, two different versions with two different aerosol treatments, bulk and modal, were used. All models have full atmosphere-ocean-land coupling as well as an explicit aerosol treatment and stratospheric chemistry. A brief description is provided below for all of the models, and a discussion of the differences in the aerosol treatments of particular importance for this work is given at the end of this section.

2.1 CESM2-WACCM6

The Community Earth System Model, version 2, with the Whole Atmosphere Community Climate Model version 6 (CESM2-WACCM6, Gettelman et al. (2019); Danabasoglu et al. (2020), hereafter CESM2) is used with a comprehensive stratospheric and upper atmospheric chemistry and interactive aerosol microphysics using the Modal Aerosol Module (MAM4) (Liu et al., 2016). It's horizontal resolution is 1.25° longitude by 0.9° latitude, with 70 vertical levels and a model top at about 140 km. An evaluation of the model response to past volcanic eruptions was performed in Mills et al. (2017) and Schmidt et al. (2018) using the previous version of the model, CESM1(WACCM). Unlike the CESM2 version described in Danabasoglu et al. (2020), which includes both comprehensive tropospheric and stratospheric chemistry, the version used here includes comprehensive stratospheric chemistry but only a simplified chemistry of importance in the troposphere; this is thus similar to the chemistry scheme in the CESM1(WACCM) version used for the previous geoengineering studies, e.g. Tilmes et al. (2018a)).

2.2 GISS-E2.1-G

NASA's ModelE is developed by the Goddard Institute for Space Studies (GISS). The current version, ModelE2.1, has a horizontal resolution of 2.5° longitude by 2° latitude and 40 vertical layers extending up through the mesosphere (model top of ∼80 km). The version used in this study, GISS-E2.1-G, has a fully interactive ocean with 32 vertical layers, based on the Russell ocean (Kelley et al., 2020). While GISS ModelE also has the ability to use the HYCOM ocean (Kelley et al., 2020), that option is not employed here. GISS has two methods of representing aerosol microphysics that we employed here. The bulk aerosol treatment (referred to as One-Moment Aerosol, OMA in CITE, called 'GISS bulk' in this study) involves specification of an aerosol dry radius, and the aerosols grow hygroscopically as a function of the relative humidity (Koch et al., 2006). The modal aerosol treatment (referred to as Multiconfiguration Aerosol TRacker of mIXing state, MATRIX in Bauer et al. (2008), called 'GISS modal' in this study) involves computation using quadrature of moments and can represent aerosol microphysical growth via condensation and coagulation. Both aerosol methods have a representations of heterogeneous halogen chemistry on the aerosol surfaces. For anthropogenic, tropospheric aerosols, a comparison between the two aerosol treatments in GISS is presented in Bauer et al. (2020).

https://doi.org/10.5194/egusphere-2022-401
Preprint. Discussion started: 13 June 2022

2.3 UKESM1.0

The UKESM1 Earth system model (Sellar et al., 2019) was developed jointly by the UK's Met Office and Natural Environment Research Council and consists of the physical atmosphere-land-ocean-sea-ice coupled model HadGEM3-GC3.1 (Kuhlbrodt et al., 2018) coupled to components which deal with terrestrial and ocean biogeochemistry (Wiltshire et al., 2021; Yool et al., 2021) and atmospheric composition and aerosols via the UKCA module (Archibald et al., 2020; Mulcahy et al., 2018; Mann et al., 2010; Walters et al., 2019). The horizontal resolution is 1.875° longitude × 1.75° latitude, with 85 vertical levels up to ≃84 km on terrain-following hybrid height coordinate. An evaluation of simulations of past volcanic eruption has been recently performed in Dhomse et al. (2020) for on older version of this model using a similar version of the aerosol scheme.

2.4 Differences between the aerosol microphysics schemes used

None of the models used in this study employ a sectional aerosol microphysics, where the size domain is divided into intervals, or bins, and the evolution of the number concentrations in each size bin is calculated separately for each species. Instead, these models employ a more simplified approach, either modal, where the aerosol population is described by a number of log-normal distributions, or bulk, where the size distribution is prescribed; we will describe both briefly below.

CESM2 and UKESM1 use a very similar modal approach, where the aerosol population is described by at least three main modes (at least for sulfate) called Nucleation (only for UKESM1), Aitken, Accumulation and Coarse, whose distribution is assumed to be lognormal with a fixed geometric standard deviation σ_g and a geometric mean diameter that can vary between a certain predefined size range: particle number and mass are transferred to the larger mode when the diameter exceeds the upper limit for that mode. In each mode, all aerosol species are considered internally mixed, that is, they are described by a single size distribution; this has been shown to lead to changes in upper tropospheric aerosol concentrations when large quantities of stratospheric sulfate settle down, unrealistically reducing the size distribution and thus the settling velocities of species that shouldn't interact with the sulfate (Visioni et al., 2022).

The GISS in its bulk version incorporates a much simpler aerosol parametrization, where the size distribution is specified for each aerosol species. There is no calculated number concentration and water uptake effects is solely dependent on relative humidity for gravitational settling purposes. The GISS modal version sits in between the complexity of the other two models and GISS bulk: the sulfate population is described by two lognormal distributions (Aitken and Accumulation) of fixed σ_g, but separated from other aerosol species, defined as particles with a diameter smaller or larger than 0.1 μm respectively. Instead of tracking the size distribution itself, however, only key moments of the aerosol population such as number and mass are tracked, based on the quadrature method of moments framework described in McGraw (1997), leading to a set of equations to be solved for each population described in detail in Bauer et al. (2008). Condensational growth leading to a transfer between Aitken and Accumulation modes is also treated differently than in the other two models. For a straightforward comparison, all information for the aerosol populations in each model is described in Table 1. For GISS bulk, the only prescribed value is the

https://doi.org/10.5194/egusphere-2022-401
Preprint. Discussion started: 13 June 2022

Table 1. Values for the size range (diameter, D, in μm) and geometric standard deviation σ_g for sulfate of each of the modes (when applicable) for the four participating models. Information collected from Koch et al. (2006) for GISS bulk, Bauer et al. (2008) for GISS modal, Walters et al. (2019) for UKESM and Liu et al. (2012) with integrations from Mills et al. (2016) for CESM2. All diameter are considered here as dry, as models calculate water uptake afterward depending on local humidity.

Mode name	CESM2 size (μm)	CESM2 σ_g	GISS bulk size (μm)	GISS bulk σ_g	GISS modal size (μm)	GISS modal σ_g	UKESM1 size (μm)	UKESM1 σ_g
Nucleation	-	-	-	-	-	-	D<0.01	1.59
Aitken	0.015<D<0.053	1.6	-	-	D<0.1	1.6	0.01<D<0.1	1.59
Accumulation	0.058<D<0.48	1.6	0.3 (fixed)	NA	D>0.1	1.8	0.1<D<0.5	1.40
Coarse	D>0.4	1.2	-	-	-	-	D>0.5	2

bulk radius (which for simplicity we included in the Accumulation row in the table) with no assumptions over the geometric standard deviation; the actual value of 0.15 μm is different from the one given in Koch et al. (2006) (0.2 μm).

3 Experimental protocol

3.1 Baseline emission scenario

For these experiments, we selected the baseline Shared Socioeconomic Pathway (SSP) 2-4.5 (Meinshausen et al., 2020). Each experiment is run for 10 years starting on January 1^{st} 2035. The choice of a particular background scenario is of secondary importance here, as all comparisons of the SAI responses will be performed relative to the control SSP2-4.5 simulation, thereby evaluating climate changes due to solely the increased sulfate aerosol concentrations. However, in planning for future, more comprehensive experiments (as those detailed in Richter et al. (2022) and MacMartin et al. (2022)) we use a similar background greenhouse gas scenario.

3.2 Specifics for the SO_2 injection

In the experiments discussed in Tilmes et al. (2017), the altitudes of SO_2 injections were defined in terms of a fixed height above the annual mean tropopause. This led to two different injections altitudes, one for 15°N and 15°S injections at 25.0 km and one for injections at 30°N and 30°S at 22.4 km. Here we define a single injection altitude for all latitudes at 22 km. We chose this injection altitude for two reasons. First, it is closer to the upper limit of altitudes achievable by traditional aircraft (Smith, 2020) while still being sufficiently far above the tropopause for aerosols not to be removed too quickly (as opposed to 25 km, which is likely too high for practical considerations). Second, we aimed to inject SO_2 in all models at the same latitude but also in just one gridbox; however, there is a challenge in prescribing a fixed injection altitude in kilometers but having a hybrid height vertical coordinate (UKESM1) or a hybrid sigma-pressure coordinate (CESM2, GISS). And so the

https://doi.org/10.5194/egusphere-2022-401
Preprint. Discussion started: 13 June 2022

choice of 22 km ensured that all three models could always be reasonably expected to inject in the same gridbox. In CESM2, this meant injecting at the gridbox bounded by the 47 hPa and 39 hPa pressure interfaces (with a midpoint of 43 hPa), which has an average geometric height of 21.6 km at all considered latitudes of injection and is 1.2 km thick. In UKESM1, this meant injecting at the level with a midpoint height of 21.8 km, which is roughly 1 km thick. In GISS, this meant injecting at the gridbox bounded by the 43 and 31 hPa interfaces, with an approximate midpoint of 37 hPa (23.1 km assuming a 7 km scale height) and approximately 2.3 km thick.

SO_2 is injected continuously throughout the year in the same quantity in each experiment: each simulation includes the injection in only one location, either 30°N, 15°N, 0°N, 15°S or 30°S, and at one longitude (180°E for GISS and CESM2, 0°E for UKESM1) at the altitude described above. Simulations are performed for 10 years each. The selected SO_2 injection rate in each model is 12 Tg-SO_2 per year, to allow for an easier comparison with past simulations with CESM1-WACCM in Tilmes et al. (2017).

4 Results

4.1 Changes in stratospheric aerosols

Fig. 1 shows the evolution of the global mean changes in stratospheric Aerosol Optical Depth (AOD, calculated for all models at 550 nm) and surface temperatures. A relatively good agreement is found between the CESM2, GISS modal and UKESM1 in terms of the global mean AOD responses, whereas the global mean temperature response is similar for CESM and UKESM1, and for the two GISS versions separately. GISS bulk presents AOD values larger than the other two models and GISS modal, with differences ranging from values that are two times larger (for equatorial and 15°N injections) to 33% larger (for 30°N injections). Larger values of sulfate burden can result in a number of non-linear effects (Niemeier and Timmreck, 2015), for instance on atmospheric dynamics and thus the latitudinal aerosol distribution (Visioni et al., 2020) or on surface climate (Simpson et al., 2019; Jiang et al., 2019). However, considering the aim of these simulations is to inform future simulations like those described in (Kravitz et al., 2017), where the amount of SO_2 injected is determined each year in order to achieve some specified surface temperature goals, the ratio of SO_2 injected to AOD produced is less important as the injection rate can be adjusted to achieve a desired AOD.

Figure 2 shows the latitudinal distributions of the simulated stratospheric AOD. The inter-model spread is different depending on the injection location, both in terms of overall magnitude and in terms of the spatial distribution. Equatorial injections show by far the greatest differences, with UKESM1 simulating twice as much AOD in the tropics compared to CESM2, and the two GISS versions differing by up to a factor of 5 between each other. Similar differences between UKESM1 and CESM2 have also been documented for the GeoMIP G6 experiment in Jones et al. (2021). Part of these differences are driven by differences in the global mean values of AOD: as mentioned above, AOD in GISS bulk is over two times larger than in GISS modal for the equatorial injection case. For this reason, in the right panels of Figure 2 the zonal mean AOD values are scaled by the respective

https://doi.org/10.5194/egusphere-2022-401
Preprint. Discussion started: 13 June 2022

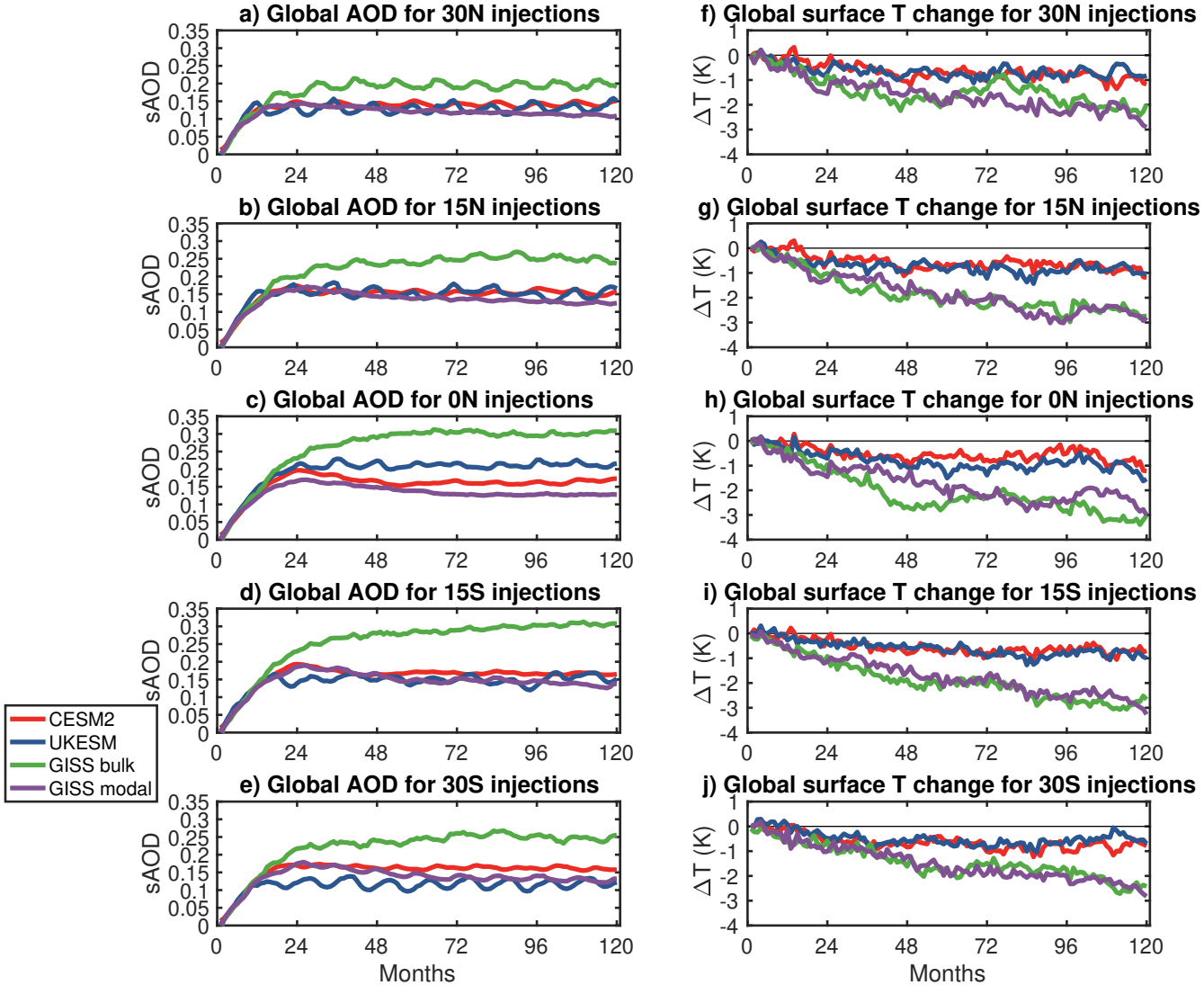

Figure 1. Timeseries of global mean monthly mean changes in stratospheric AOD (a-e) and surface temperature (f-f) resulting from the single-point injections at 30°N (a, f), 15°N (b, g), 0°N (c, h), 15°S (d, i) and 30°S (e, j) compared to the corresponding baseline SSP2-4.5 simulation in each of the models.

https://doi.org/10.5194/egusphere-2022-401
Preprint. Discussion started: 13 June 2022

global mean values; this highlights the differences in the latitudinal distribution of the responses. This way, the difference in the normalised magnitudes of the equatorial peak (defined here as the average between 5°N and 5°S) between CESM2 and UKESM1 is reduced from 1.8 to 1.4; and similarly the two GISS versions show much more similar results, especially in the tropical region . In general, injections in the Southern Hemisphere (SH) show larger inter-model differences compared to the Northern Hemisphere (NH) injections, especially at high latitudes. In the 30°S case, global mean values are more than twice as large in GISS bulk (0.25) compared to UKESM1 (0.12), and the SH high-latitudinal AOD differs by a factor of three. In the NH, the largest difference is 60% between UKESM1 (0.12) and GISS bulk (0.20) in the 30°N case, and high-latitudinal AOD differs by a factor of two. When normalised, the differences are largely reduced, but a clear differentiation remains for UKESM1 which show a larger tropical confinement of aerosols than the other models. There are also some notable differences in the interannual variability between models: while both GISS versions and CESM2 have a standard deviation that range between 1 and 5% of the mean values (depending on the precise latitude), UKESM1 shows a much larger variability (up to 33 % in the 30°N injection case at 60°N-90°N). In future, longer, simulations, this observation would need to be considered when considering also the interannual variability of the surface changes.

The differences in AOD can be better understood by looking at the changes in aerosol mass mixing ratios (Figure 3) and the overall sulfate column burden (Figure 4). Compared to the other models, UKESM1 shows a much stronger confinement of the aerosol mass in the tropical pipe (for equatorial injections, the peak is 1.5 μg/kg-air, whereas it is 1.1 μg/kg-air for CESM2 and GISS bulk, and 0.5 for GISS modal), and far less transport in the opposite hemisphere for both 15° injections. On the other hand, CESM2 shows a much stronger poleward transport of sulfate aerosols, as indicated by aerosol values twice as large for 30° injections compared to other models considering values above 60° in latitude.

GISS bulk also shows a larger poleward transport in all cases, but the underlying cause for this might be different between GISS and CESM2. As analyzed in depth in PART2, the baseline stratospheric dynamics is very similar between the two GISS realizations and, hence, the differences in the overall aerosol distribution can't be found there. Analyses of the stratospheric aerosol surface area density (SAD, shown in PART2 due to its importance for stratospheric ozone chemistry) indicates a far larger number of particles in GISS compared to the other models. The SAD in GISS bulk is three times as large poleward of 60° compared to CESM2, even for mass values that only differ by 30% (for instance, in the 30°N injection case). GISS bulk simulates much smaller particles (the prescribed bulk dry radius is 0.15 μm) that imply higher residence times, as gravitational settling is much lower (Visioni et al., 2022), and so the particles are more easily transported towards the pole even in the presence of a similar dynamical regime as compared with the other GISS realization. The presence of aerosols at higher altitudes even close to the poles (where the large-scale circulation should be transporting aerosols downward) further supports this observation. Smaller aerosols are also more efficient scatterers, explaining why the optical depth differences are larger than the mass differences.

https://doi.org/10.5194/egusphere-2022-401
Preprint. Discussion started: 13 June 2022

Finally, panels f-h in Figure 4 give an overview for all cases of the ratio between the overall mass of the produced aerosols (shown alone in panel 4f) and the injected amount of SO_2 (panel 4g, where the sulfate lifetime is calculated). Obviously all models show larger amounts of mass for injections closer to the equator, due to the tropical confinement increasing the aerosols lifetime. This effect is less noticeable for GISS bulk, which shows far less confinement. However, models show a distinct difference in the ratio between overall mass of SO_4 and resulting AOD (panel 4g): this indicates substantial inter-model differences in the average size of the aerosol, with obvious consequences for the efficiency of the cooling that we will analyze next.

A comparison of the effective radius (R_{eff}) is shown in Figure 5. The values for R_{eff} are indirectly derived for all models as R_{eff} is not a direct output for either UKESM1 and GISS. Therefore, we use the common available output of mass mixing ratio (χ) and number concentration (N) for each mode in each model to derive the mean radius r_i. We calculate the mean volume v_i using

$$v_i = \frac{\chi_i}{\rho_{sulfate} * N_i} \tag{1}$$

where $\rho_{sulfate}$ is the density of sulfate as considered in each model in kg/m^3 (usually 1770 kg/m^3 as in Liu et al. (2012)). The mean radius is then derived considering that the aerosol population is assumed to be a lognormal distribution with a geometric standard deviation σ_g, and is thus connected to the mean volume by

$$v_i = \frac{4}{3} * \pi * r_i^3 * exp(\frac{9}{2} * ln^2(\sigma_g)) \tag{2}$$

Finally, R_{eff} is calculated considering the definition

$$R_{eff} = \frac{\sum_i r_i^3 N_i}{\sum_i r_i^2 N_i} \tag{3}$$

where i is the number of modes considered, so 3 for CESM2 (all modes relevant to sulfate in MAM4, Liu et al. (2016)), 4 for UKESM1 and 2 for GISS modal. The single radii for each mode are shown in the Supplementary Material in Fig. Sx. The validity of our derivation is ensured by the comparison of the derived values of R_{eff} in CESM2 and the ones obtained as a direct output from the CESM2 simulations (not shown); while the off-line derivation leads to slightly smaller R_{eff} values than calculated online in the model, the overall results are similar enough for a confident comparison. A number of important features become apparent: the population-weighted radius GISS modal is almost always larger than the GISS bulk one, confirming our observation over the differences in high latitudinal concentration. CESM2 also presents a radius always larger than the GISS modal and UKESM1 one, which explains most of the discrepancies between AOD and column mass between the CESM2 and GISS models: even if CESM2 shows larger mass concentrations, smaller particles such as those in GISS are more efficient scatterers, thus GISS AOD is more comparable to CESM2. If dynamics were similar between the two models, one would also expect less mass in CESM2 compared to GISS due to reduced lifetime caused by the increased gravitational settling, but in this case, the dynamical differences dominate in determining the final concentrations. UKESM1 has intermediate

https://doi.org/10.5194/egusphere-2022-401
Preprint. Discussion started: 13 June 2022

radii between CESM2 and GISS modal.

Looking at the mean radii for each mode (Figure S1), differences in the microphysical approaches become more evident between the models, also based on the values given in Table 1. Given that UKESM1 defines the Coarse mode as particles larger than 0.5 μm, all of the stratospheric aerosols are found in the Accumulation mode (as they are in GISS), whereas CESM2, that defines the Coarse mode threshold at around 0.4 μm simulates most of the sulfate aerosols in that mode, and very few in the Accumulation mode. This particular observation shouldn't significantly influence the aerosols' behavior in the stratosphere, since the coagulation and condensation processes happen in all modes. It could, however, have some impacts on the tropospheric interactions of sulfate with cloud nuclei; for instance some models (such as CESM2) treat Coarse mode and Accumulation mode aerosols differently when calculating, for instance, the presence of heterogeneous and homogeneous ice nuclei (see for instance Visioni et al. (2022) for a discussion of undesired side effects this might have on ice nucleation rates in the upper troposphere in CESM1(WACCM)).

https://doi.org/10.5194/egusphere-2022-401
Preprint. Discussion started: 13 June 2022

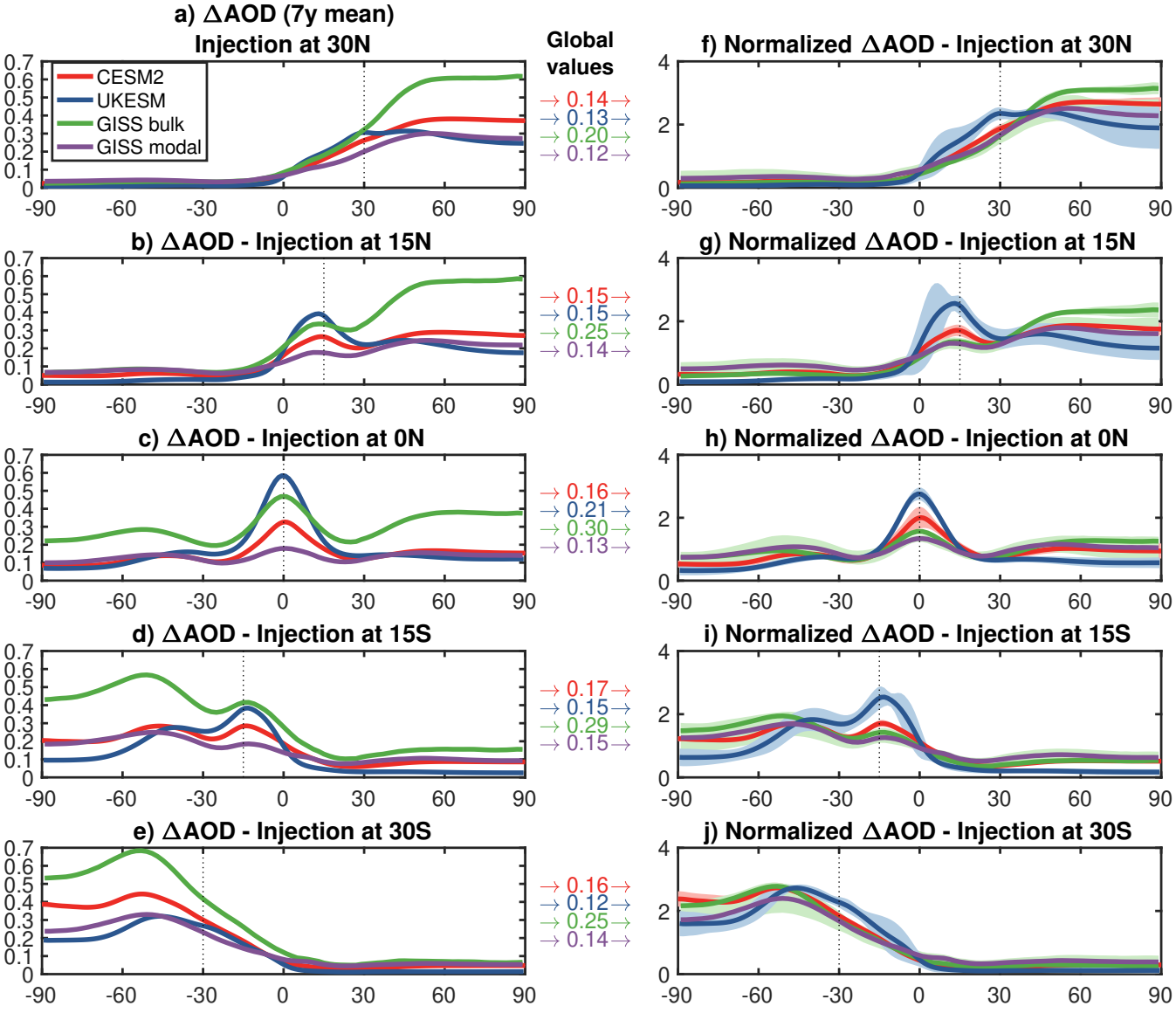

Figure 2. (a-e) Zonal and annual mean increase in stratospheric AOD resulting from single-point injections at 30°N (a), 15°N (b), 0°N (c), 15°S (d) and 30°S (e), averaged over the last seven years of simulation. (f-j) Zonal mean increase normalized to the global value of AOD in each simulation in the respective experiment; shading of the same color represent the internal variability (1 σ standard deviation) over the same period of time. For each experiment, the global mean value used in the normalization is reported between the panels on the left and right. Dashed vertical lines indicate the locations of the SO_2 injections.

https://doi.org/10.5194/egusphere-2022-401
Preprint. Discussion started: 13 June 2022

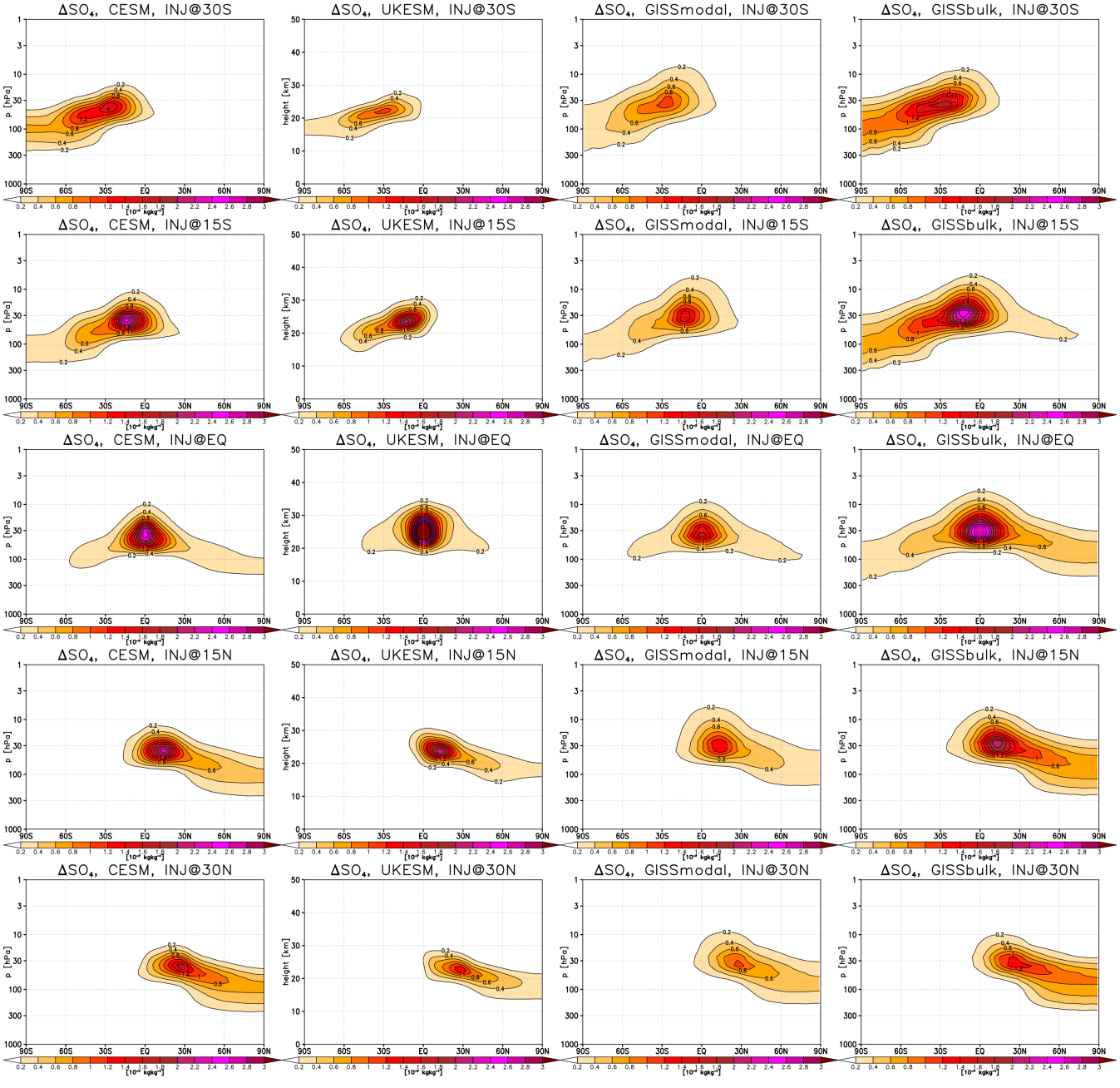

Figure 3. Zonal and annual mean increase in SO_4 mass mixing ratio (in 10^{-7}kg-SO_4/kg-air) for CESM2 (first column), UKESM1 (second column), GISS modal (third column) and GISS bulk (fourth column) and all injection locations, 30°S (first row), 15°S (second row), 0°N (third row), 15°N (fourth row) and 30°N (fifth row).

https://doi.org/10.5194/egusphere-2022-401
Preprint. Discussion started: 13 June 2022

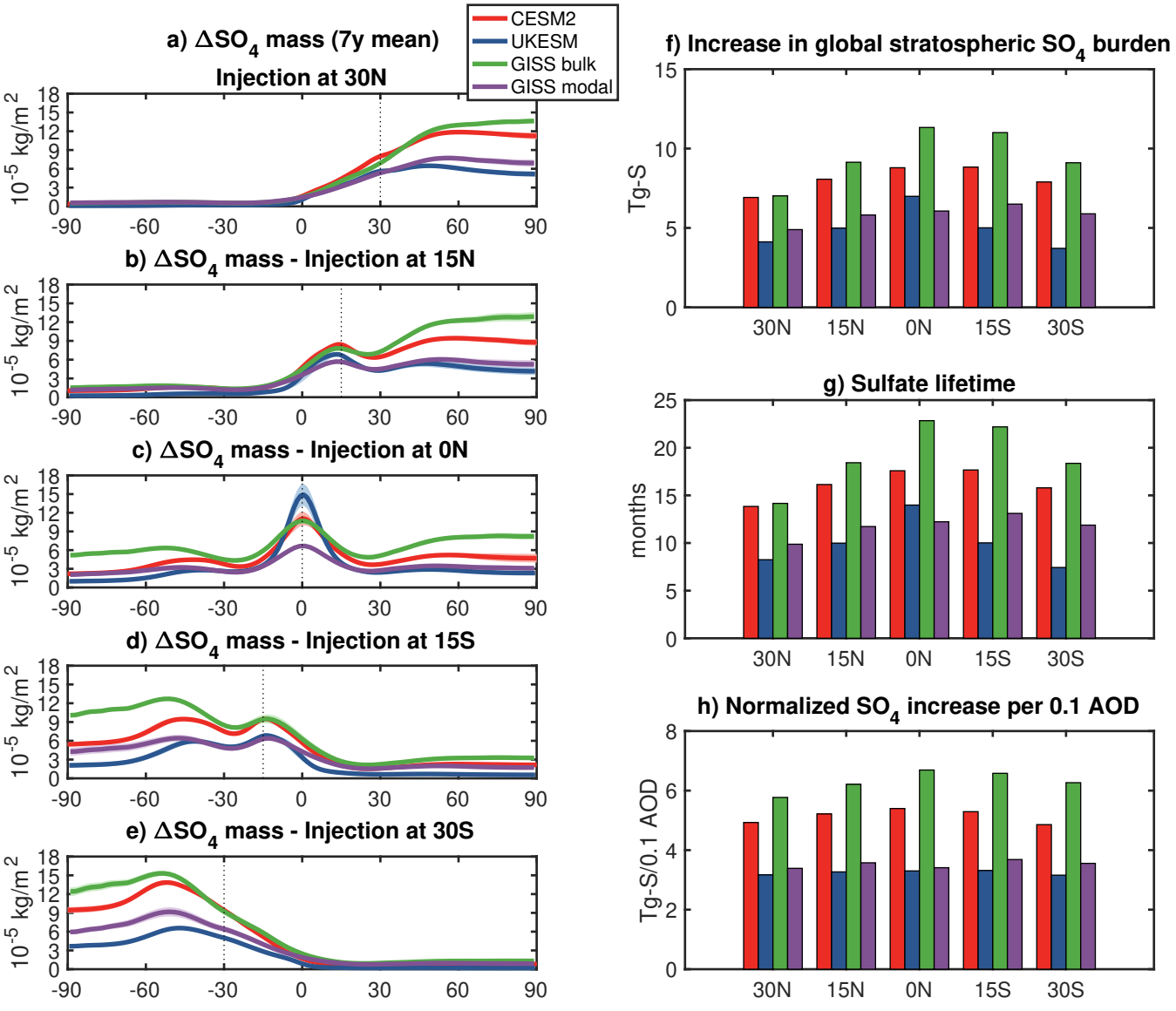

Figure 4. (a-e) Zonal and annual mean increase in total SO_4 column burden for each experiment, 30°N (first row), 15°N (second row), 0°N (third row), 15°S (fourth row) and 30°S (fifth row). f) Total global increase in stratospheric sulfate burden (in Tg-S). g) Stratospheric sulfate lifetime (in months) h) Global increase in column sulfate burden, normalized by the obtained global mean increase in stratospheric AOD.

https://doi.org/10.5194/egusphere-2022-401
Preprint. Discussion started: 13 June 2022

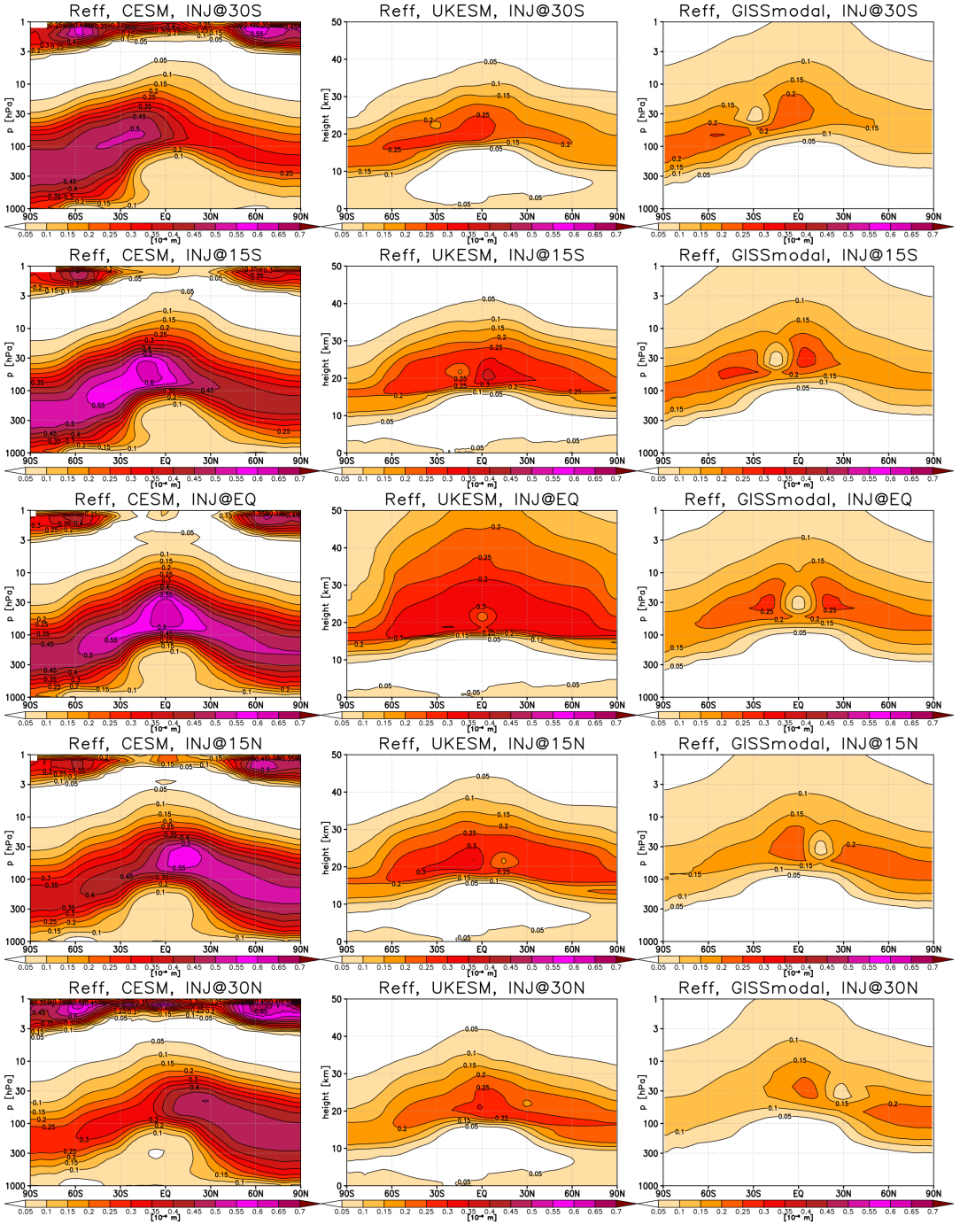

Figure 5. Effective radius (in 10^{-6} m) in CESM2 (left), UKESM1 (center) and GISS modal (right) simulations for each experiment, 30°S (first row), 15°S (second row), 0°N (third row), 15°N (fourth row) and 30°N (fifth row).

https://doi.org/10.5194/egusphere-2022-401
Preprint. Discussion started: 13 June 2022

The resulting zonal mean cooling achieved by the AOD increase in each simulation is shown in Figure 6, including both the absolute temperature changes and values normalized by the global means. Differences between models are still evident, but a direct correlation with the AOD changes in Fig. 2 is not present; for instance, the general temperature responses between the two GISS realizations are much more similar than their simulated AOD. This is because temperature responses compound many sources of uncertainty, including not only those related to the magnitude and spatial pattern of the simulated stratospheric AOD (thus related to the model microphysics and transport), but also to the resulting radiative and thermodynamical processes in the troposphere that determine how much cooling AOD produces and how the regional patterns of cooling differ. We find very large differences between the models in the magnitude of the global mean cooling per unit AOD (Figure 7). CESM2 and UKESM1 show, on average, 4.7 K and 5.4 K cooling per unit of AOD, respectively. This is roughly in line with the multi-model average of GeoMIP G6sulfur experiment (4.6 K per unit AOD for injections between 10°N and 10°S in GeoMIP (Visioni et al., 2021), compared to the 3.9 K and 4.8 K cooling per unit AOD in CESM2 and UKESM1, respectively, for the equatorial injections here). In contrast, the GISS models show significantly larger cooling per unit AOD, with 8.6 K on average in GISS bulk and 16.7 K on average in GISS modal; the latter is more than three times as high as in CESM2. This large difference is not primarily due to differences in the global cooling produced between the two GISS realizations, but rather due to the much smaller amount of AOD simulated in GISS modal; the smaller AOD in GISS modal results in a similar level of surface cooling as is simulated in GISS bulk under much larger AOD values. The cause for the discrepancies between the two GISS realizations is most likely found in similar tuning procedures for the model (described for GISS-E2.1 in Kelley et al. (2020)); while these mainly target the global radiative balance, they often also try to constrain the aerosol forcing (this is described for instance in Schmidt et al. (2017), where both GISS and CESM1 tuning procedures are explained in some detail). The two GISS versions used here show large differences in the baseline aerosol optical depth from sulfate: in the mid-latitudinal NH, where anthropogenic sulfate aerosol production is maximized, GISS modal shows on average a 0.03 AOD, just like CESM2, while GISS bulk shows on average a 0.11 AOD (see Figure S2). It is thus plausible that in order to compensate for this difference during the tuning, the sensitivity to aerosols in the modal version of GISS has been increased, explaining why a much smaller stratospheric AOD produces a similar surface cooling to the one in GISS bulk. We note that this reasoning can't be generalized to find an explanation for all inter-model differences, but it is a reasonable hypothesis in this case for the two GISS models that share the same dynamics and model physics otherwise. It is also possible that the differences in global cooling in GISS may depend on the substantial tropospheric ozone depletion observed in the two models in PART2, which would influence the global forcing, and that it is not present in CESM2 and UKESM.

The normalized values in the right panels of Figure 6 show some level of consistency in the temperature response amongst the models. In particular, the models agree that equatorial injections tend to cool the NH more than the SH, and that the cooling produced by the NH injections is strongest in the NH (this is particularly marked in CESM2 for the 15°N injection), whereas the cooling produced by the SH injections is more evenly distributed between the two hemispheres. In contrast, the models tend to disagree with respect to responses in the NH high latitudes; this is unlike in the SH high latitudes, which can be understood by the role of dynamical atmospheric and sea-ice variability in contributing to the responses in this region (Banerjee et al.,

https://doi.org/10.5194/egusphere-2022-401
Preprint. Discussion started: 13 June 2022

2020).

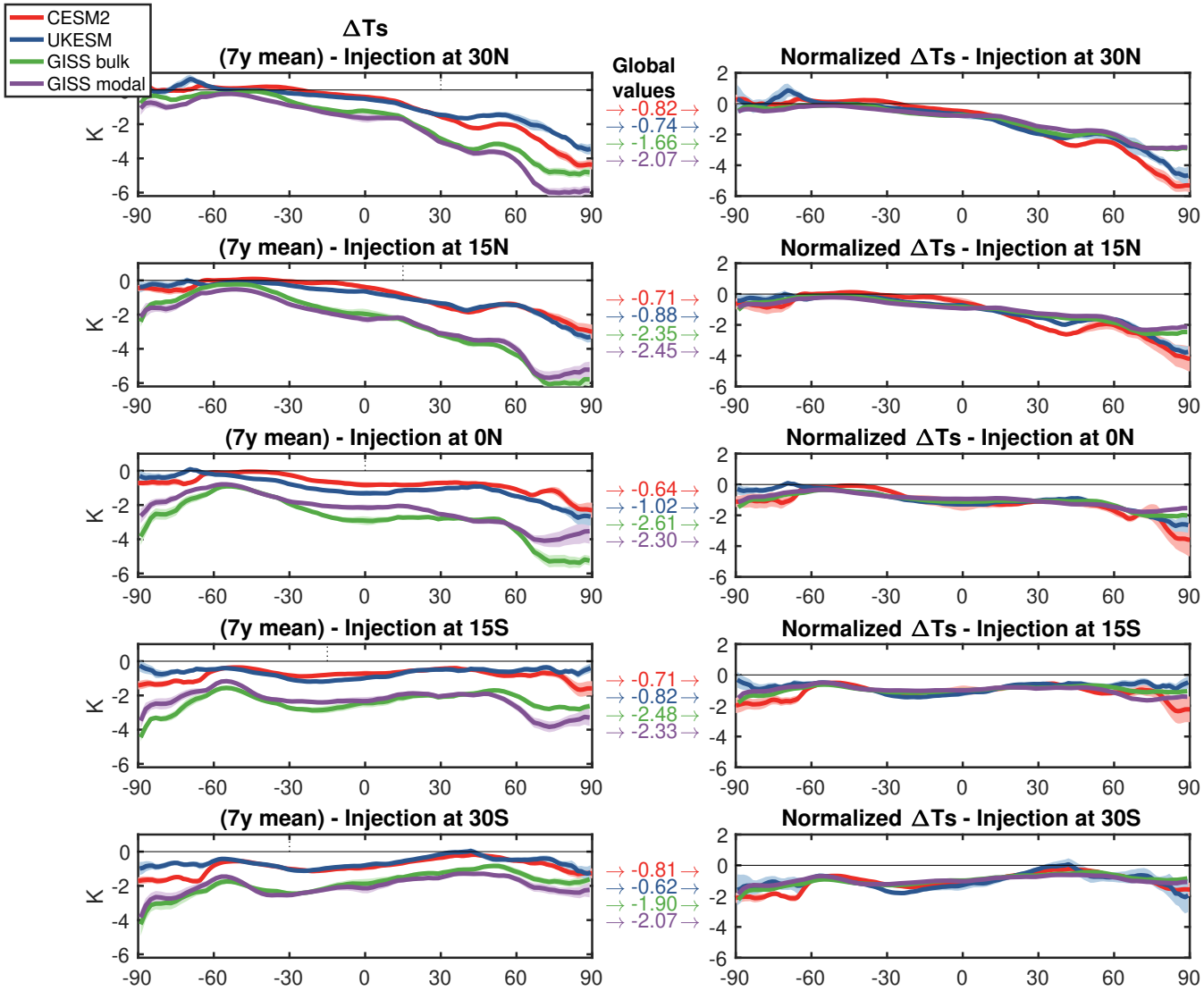

Figure 6. (a-e) Zonal and annual mean change in surface temperatures (K) resulting from the single-point injections at either 30°N (a), 15°N (b), 0°N (c), 15°S (d) or 30°S (e), averaged over the last seven years of simulation. (f-j) Zonal mean changes normalized with the corresponding global mean values in each experiment; shading of the same color represent the interannual variability (1 σ) over the same period of time. For each experiment, the global mean value used in the normalization is reported between the panels on the left and right.

https://doi.org/10.5194/egusphere-2022-401
Preprint. Discussion started: 13 June 2022

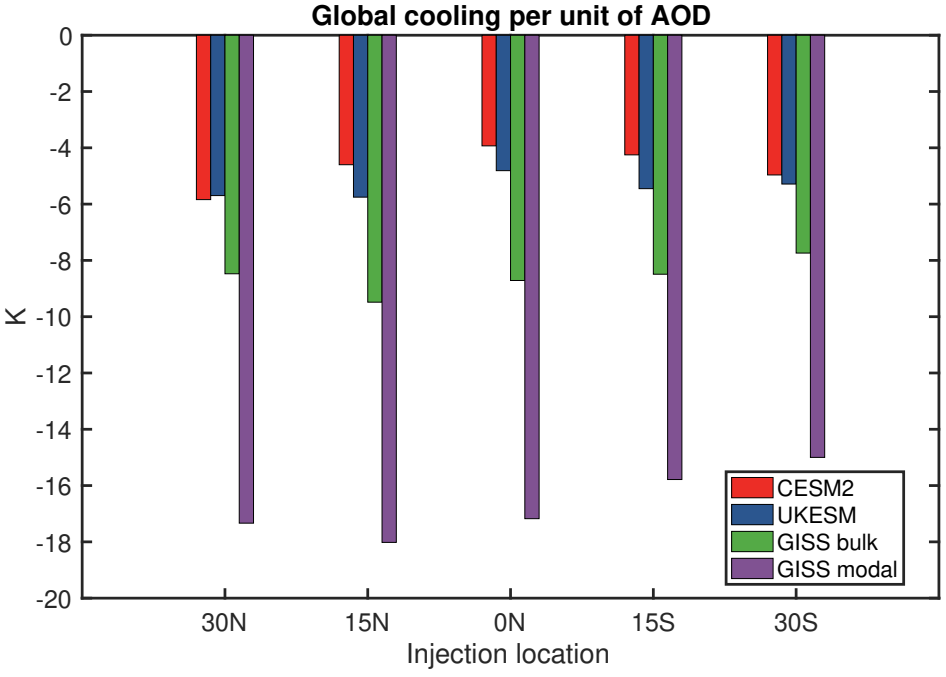

Figure 7. Global mean cooling achieved in each experiment and injection location per unit increase in the associated global mean stratospheric AOD.

https://doi.org/10.5194/egusphere-2022-401
Preprint. Discussion started: 13 June 2022

Finally, in Figure 8 we show the zonal mean changes in precipitation. In this case, we show both the magnitude of the change in mm/day, and the corresponding % changes with respect to the baseline precipitation pattern in each model. In general, precipitation changes depend on even more factors than temperature changes (Kravitz et al., 2013; Tilmes et al., 2013). Differences in the inter-hemispheric cooling patterns produce different shifts in the precipitation response by moving the intertropical convergence zone (ITCZ) (Haywood et al., 2013), and this is compounded with differences in the clouds responses (Smyth et al., 2017) and in the large-scale dynamical changes resulting from the aerosol-induced stratospheric heating (Simpson et al., 2019). Furthermore, the modeled responses is also regionally dependant: while the precipitation response to SAI in the G6 GeoMIP simulations shows consensus in some regions such as the increases in December-January-February precipitation over northern Europe and decreases over southern Europe in response to a forced positive North Atlantic Oscillation, the same models show little consensus over the North American continent (Jones et al., 2022).

The precipitation response also depends on the climatological precipitation, which differs more between the models than the climatological temperature does (not shown). We find a general qualitative agreement between the models in the tropics. All models show shifts in tropical precipitation depending on the hemisphere of injection, with decreased precipitation in that hemisphere and increased precipitation in the opposite one. The equatorial injections in turn result in an overall reduction of tropical precipitation. Changes at mid and high latitudes, which are much smaller in absolute terms than those in the tropics, can be as high in terms of percentage changes as those in the tropics, but the models disagree on the sign and magnitude of the responses there far more than they do in the tropics.

Changes in the precipitation patterns discussed above can be also understood by looking at changes in the ITCZ (Fig. 9), which we define here as the latitude near the equator where the meridional mass streamfunction at 500 hPa changes sign. The model agreement in the simulated ITCZ shifts is even more evident, despite the significant differences in the climatological ITCZ locations. The larger simulated ITCZ shifts for the NH injections compared to the SH injections are also consistent with the different cooling patterns, with stronger and more NH-confined cooling for the 30°N and 15°N injections. A similar signal in the behavior of the ITCZ is also found after volcanic eruptions both for the equatorial (Trenberth and Dai, 2007) and extra-equatorial eruptions (Oman et al., 2006).

https://doi.org/10.5194/egusphere-2022-401
Preprint. Discussion started: 13 June 2022

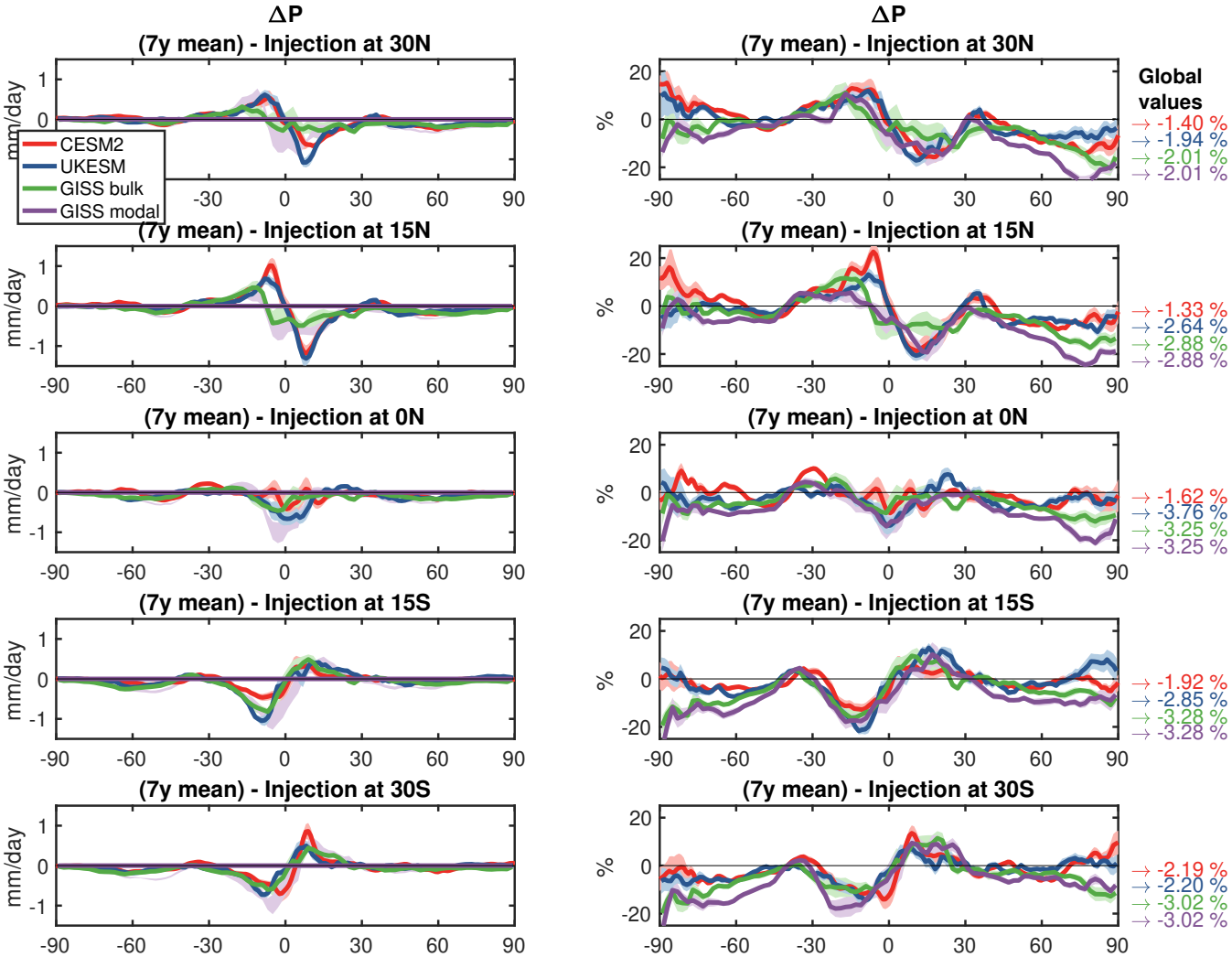

Figure 8. (a-e) Zonal and annual mean changes in precipitation (mm/day) resulting from the single-point injections at either 30°N (a), 15°N (b), 0°N (c), 15°S (d) or 30°S (e), averaged over the last five years of simulation. (f-j) As (a-e), but with percent changes obtained by normalizing to the baseline zonal mean precipitation in each model.

https://doi.org/10.5194/egusphere-2022-401
Preprint. Discussion started: 13 June 2022

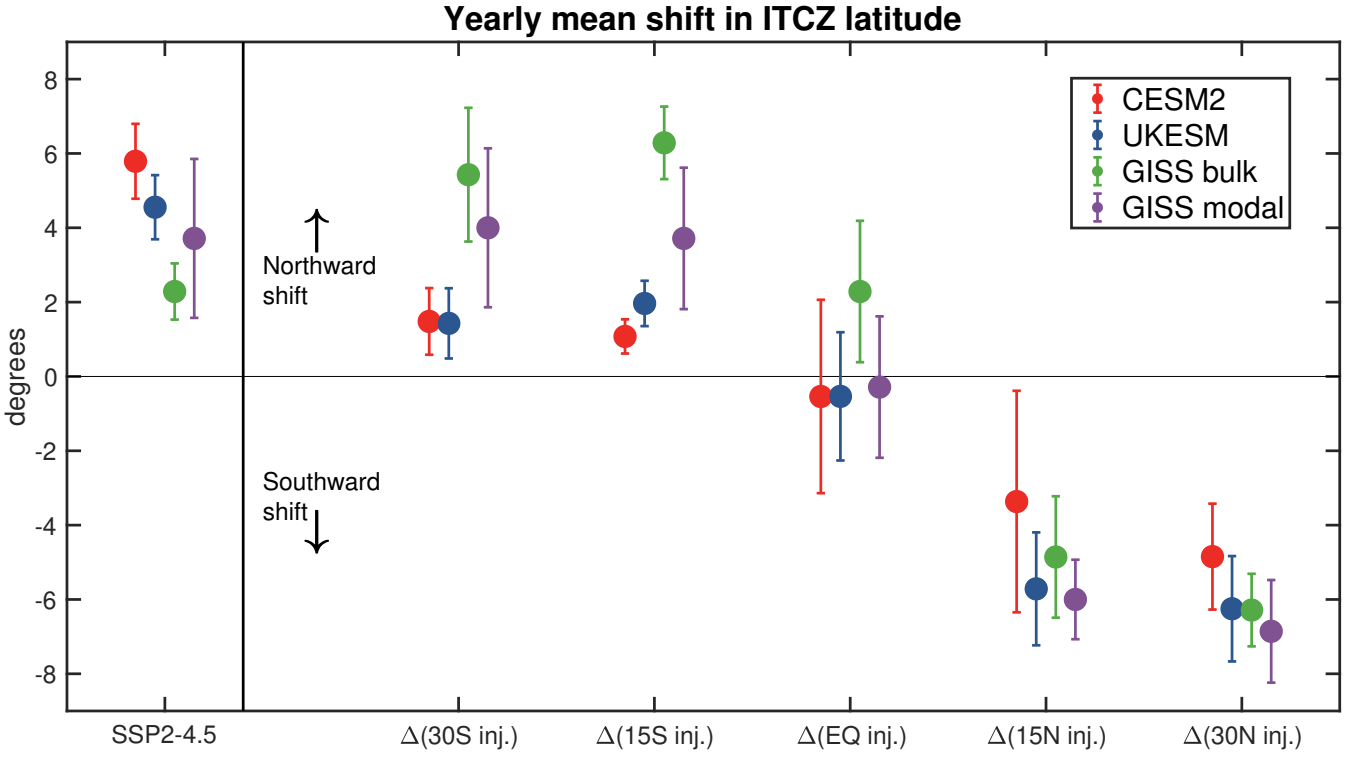

Figure 9. Annual mean changes in the latitude of ITCZ, here defined as the latitude near the equator where the meridional mass stream-function at 500 hPa changes sign (defined as the mid-point between the two gridboxes). Results are shown for each injection location (30°S, 15°S, 0°N, 5°N and 30°N) and each model. Error bars indicate the σ standard deviation for the last seven years of the SAI simulation. Shown also on the left hand side is the climatological ITCZ position in the corresponding SSP2-4.5 simulation.

https://doi.org/10.5194/egusphere-2022-401
Preprint. Discussion started: 13 June 2022

5 From single point injections to multi-target simulations: designing the feedback algorithm

One of the goals of this exercises is to reproduce in multiple climate models a similar geoengineering strategy to that described in Kravitz et al. (2017), i.e. where a feedback algorithm determines the amount of SO_2 to be injected at each year at each of the specified locations in order to achieve a set of predetermined surface temperature targets. As discussed in Kravitz et al. (2016) and Zhang et al. (2022), year-round injections at the four injection locations described here (30°N, 15°N, 15°S and 30°S) allow for the management of three independent degrees of freedom in surface temperature. Combining varying rates of injections at these four locations produces distinct patterns of AOD.

One method of describing these AOD patterns is to project the zonal mean AOD onto the first three Legendre polynomials evaluated as a function of sine of latitude. Here ℓ_0 describes the global mean, $\ell_1 = sin(\psi)$ describes the pole-to-pole gradient, and $\ell_2 = \frac{1}{2}(3sin^2(\psi) - 1)$ describes the equator-to-pole gradient. Injecting at the same time at 15°N and 15°S produces ℓ_0; injecting at 15° and 30° N (or S) produces $\ell_0 + \ell_1$ or $\ell_0 - \ell_1$, respectively; and injecting at 30°N and 30°S produces $\ell_0 + \ell_2$. Therefore, injections at these four latitudes can be combined (assuming linearity) to achieve desired combinations of L_0, L_1, and L_2, subject to the constraints $\ell_0 \geq 0$, $\ell_2 \geq 0$, and $\ell_0 \geq |\ell_1| + \ell_2$. This truncated Legendre decomposition of the zonal mean AOD into ℓ_0, ℓ_1, and ℓ_2 is not the only way to numerically define an SAI strategy, but it has been found to be sufficient to independently control three degrees of freedom in surface temperature: the global mean ($T_0 = \frac{1}{A}\int_\psi T(\psi)\cos(\psi)\mathrm{d}\psi$, controlled by ℓ_0), the pole-to-pole temperature gradient ($T_1 = \frac{1}{A}\int_\psi \sin(\psi)T(\psi)\cos(\psi)\mathrm{d}\psi$, controlled by ℓ_1), and the equator-to-pole temperature gradient ($T_2 = \frac{1}{A}\int_\psi \frac{3\sin^2(\psi)-1}{2}T(\psi)\cos(\psi)\mathrm{d}\psi$, controlled by ℓ_2). Similarly, the definition of the four injection latitudes described here is not exhaustive, in the sense that it is not the only univocal way to produce the three described aerosol patterns, as there could be other latitudes of injection that once combined could produce L_0, L_1 and L_2 with smaller residuals. Our choice is thus only intended to illustrate the optimization method.

In this section, we present the calculations necessary for this strategy to be implemented in the three climate models considered in this study; similar analyses for CESM1(WACCM) are performed and explained in detail in MacMartin et al. (2017). In order to design such a feedback control algorithm, it is first necessary to quantify the relationships between injections at each of the four latitudes ($q = [q_{30S}\ q_{15S}\ q_{15N}\ q_{30N}]^T$) and the patterns of AOD they create ($\ell = [\ell_0\ \ell_1^N\ \ell_1^S\ \ell_2]^T$, where ℓ_1^N denotes $\ell_1 \geq 0$ and ℓ_1^S denotes $\ell_1 \leq 0$), and then the relationship between AOD (ℓ) and temperature (T_0, T_1, and T_2). The first relationship can be defined by two matrices M and F such that $q = MF^{-1}\ell$. For each the four models, using the values shown in Figure 2, this relationship is computed to be as follows:

https://doi.org/10.5194/egusphere-2022-401
Preprint. Discussion started: 13 June 2022

$$
\begin{aligned}
CESM: \begin{bmatrix} q_{30S} \\ q_{15S} \\ q_{15N} \\ q_{30N} \end{bmatrix} &= \begin{bmatrix} 25\ell_1^S + 38\ell_2 \\ 39(\ell_0 - (\ell_1^N + \ell_1^S + \ell_2)) + 45\ell_1^S \\ 34(\ell_0 - (\ell_1^N + \ell_1^S + \ell_2)) + 59\ell_1^N \\ 15\ell_1^N + 43\ell_2 \end{bmatrix} \quad UKESM: \begin{bmatrix} q_{30S} \\ q_{15S} \\ q_{15N} \\ q_{30N} \end{bmatrix} = \begin{bmatrix} 56\ell_1^S + 50\ell_2 \\ 37(\ell_0 - (\ell_1^N + \ell_1^S + \ell_2)) + 22\ell_1^S \\ 36(\ell_0 - (\ell_1^N + \ell_1^S + \ell_2)) + 18\ell_1^N \\ 49\ell_1^N + 46\ell_2 \end{bmatrix} \\
GISS_{bulk}: \begin{bmatrix} q_{30S} \\ q_{15S} \\ q_{15N} \\ q_{30N} \end{bmatrix} &= \begin{bmatrix} 6\ell_1^S + 26\ell_2 \\ 23(\ell_0 - (\ell_1^N + \ell_1^S + \ell_2)) + 35\ell_1^S \\ 20(\ell_0 - (\ell_1^N + \ell_1^S + \ell_2)) + 44\ell_1^N \\ 0\ell_1^N + 29\ell_2 \end{bmatrix} \quad GISS_{modal}: \begin{bmatrix} q_{30S} \\ q_{15S} \\ q_{15N} \\ q_{30N} \end{bmatrix} = \begin{bmatrix} 38\ell_1^S + 46\ell_2 \\ 44(\ell_0 - (\ell_1^N + \ell_1^S + \ell_2)) + 47\ell_1^S \\ 39(\ell_0 - (\ell_1^N + \ell_1^S + \ell_2)) + 69\ell_1^N \\ 22\ell_1^N + 49\ell_2 \end{bmatrix}
\end{aligned} \tag{4}
$$

with q in Tg per year. These values can be obtained considering separately the injection amounts necessary to obtain the four AOD patterns described above, and solving the linear least-squares problem considering as a constraint that no negative injection, or AOD values, are possible. This is shown in Figure 10 for all models; the linear combination of the coupled injection locations in each of the four cases successfully manages to produce a pattern similar to the desired one. Models all agree on the need to deploy quasi-symmetrical amounts to obtain the ℓ_0 and $\ell_0 + \ell_2$ patterns (with at most a 20% difference in some cases) whereas they differ largely on how to obtain the $\ell_0 + \ell_1^N$ and $\ell_0 + \ell_1^S$ patterns. For instance, to obtain $\ell_0 + \ell_1^N$, CESM2 requires four times as much injection at 15°N than it does at 30°N, whereas UKESM1 requires two times as much injection at 30°N than it does at 15°N, and GISS requires no injection at 30°N at all. The residuals also show that how close the models get to the desired patterns differs, with CESM2 being twice as low as any other models in all cases. It is important to note that the results obtained with the current version of CESM2 (CESM2-WACCM6) are very similar but not identical ($< 10\%$) to those obtained and discussed in MacMartin et al. (2017) using CESM1(WACCM). In that case, injections were at different altitudes (25 km for 15°N and S, and 22 km for 30°N and S), and so some differences are to be expected.

Similarly, using the patterns of temperature response shown in Figure 6, combined with the patterns in AOD, we can derive the second relationship (between ℓ and T_0, T_1 and T_2. For the four models, this leads to

$$
\begin{aligned}
CESM: \begin{bmatrix} T_0 \\ 3T_1 \\ 5T_2 \end{bmatrix} &\simeq \begin{bmatrix} \mathbf{-4.1} & 0 & 0 \\ -3.0 & \mathbf{-3.9} & 0 \\ -1.5 & -1.6 & \mathbf{-0.5} \end{bmatrix} \begin{bmatrix} \ell_0 \\ \ell_1 \\ \ell_2 \end{bmatrix} \quad UKESM: \begin{bmatrix} T_0 \\ 3T_1 \\ 5T_2 \end{bmatrix} \simeq \begin{bmatrix} \mathbf{-4.6} & 0 & 0 \\ -2.6 & \mathbf{-3.6} & 0 \\ -0.2 & -1.5 & \mathbf{-1.3} \end{bmatrix} \begin{bmatrix} \ell_0 \\ \ell_1 \\ \ell_2 \end{bmatrix} \\
GISS_{bulk}: \begin{bmatrix} T_0 \\ 3T_1 \\ 5T_2 \end{bmatrix} &\simeq \begin{bmatrix} \mathbf{-5.6} & 0 & 0 \\ -0.9 & \mathbf{-4.4} & 0 \\ 0.7 & -1.0 & \mathbf{-4} \end{bmatrix} \begin{bmatrix} \ell_0 \\ \ell_1 \\ \ell_2 \end{bmatrix} \quad GISS_{modal}: \begin{bmatrix} T_0 \\ 3T_1 \\ 5T_2 \end{bmatrix} \simeq \begin{bmatrix} \mathbf{-9.2} & 0 & 0 \\ -4.2 & \mathbf{-6.8} & 0 \\ -1.4 & -2.4 & \mathbf{-6} \end{bmatrix} \begin{bmatrix} \ell_0 \\ \ell_1 \\ \ell_2 \end{bmatrix}
\end{aligned} \tag{5}
$$

6 Conclusions

In this work, we have shown the results of a first systematic intercomparison of climate responses to fixed single point SO_2 injections in different climate models with interactive aerosol microphysics and comprehensive stratospheric chemistry. In par-

https://doi.org/10.5194/egusphere-2022-401
Preprint. Discussion started: 13 June 2022

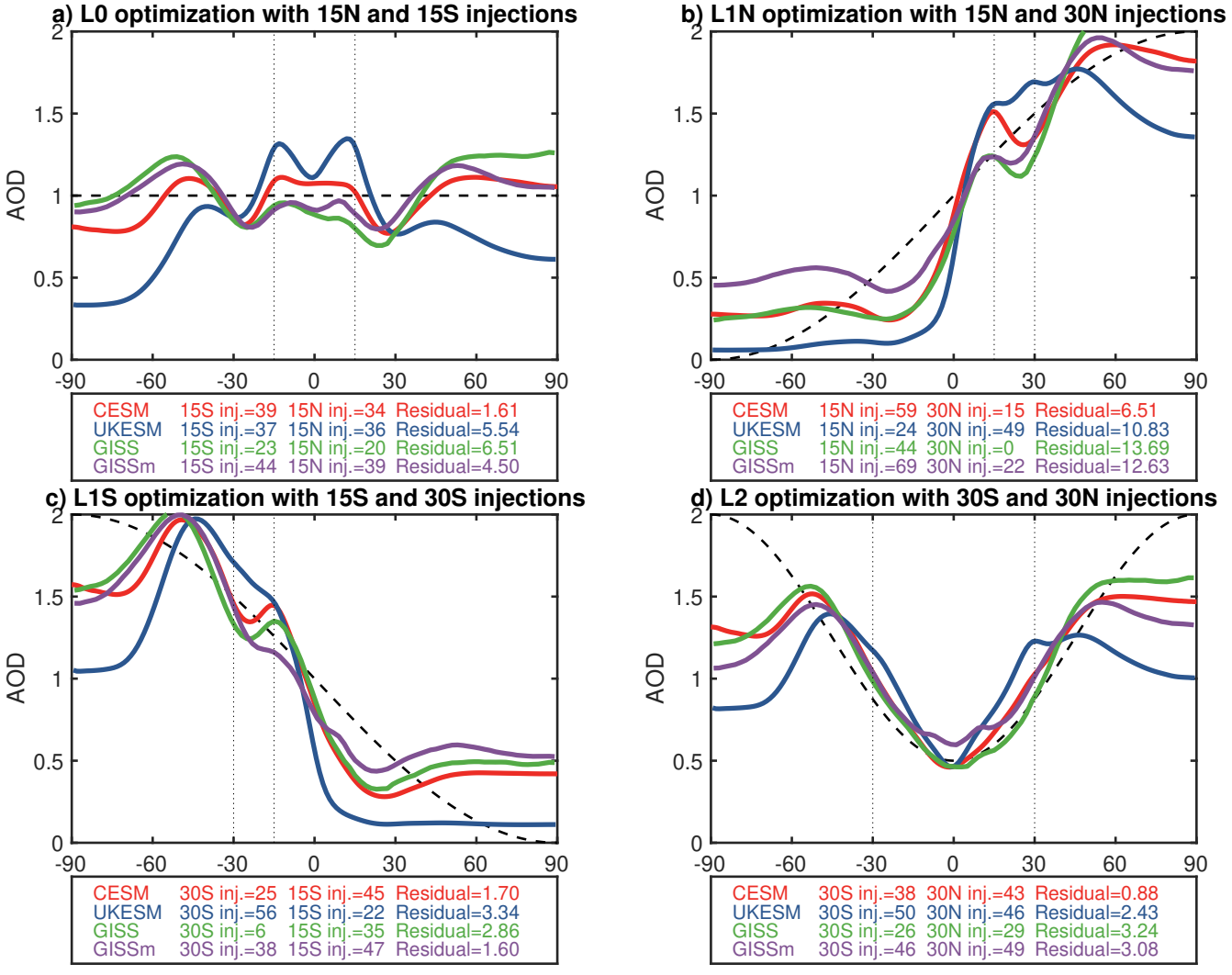

Figure 10. Linear least-squares solution to obtain an L0-shaped AOD using only 15°N and 15°S injections (a), an L0+L1 (L1N) one using only 15°N and 30°N injections (b), an L0-L1 (L1S) one using only 15°S and 30°S injections (c) and a L2 one using only 30°S and 30°S injections (d). Values at the bottom of each plot (in Tg-SO_2/yr) indicate the required injection, assuming linearity, based on the AOD distribution in Figure 2. The residual of each solution is also included.

https://doi.org/10.5194/egusphere-2022-401
Preprint. Discussion started: 13 June 2022

ticular, we used CESM2-WACCM6, UKESM1.0, GISS-E2.1-G with bulk aerosol microphysics and GISS-E2.1-G with modal aerosol microphysics, and a set of simulations injecting a fixed quantity of SO_2 at five different latitudes (30°N, 15°N, 0°N, 15°S and 30°S) and at 22 km of altitude. The same protocol was used in all models to determine similarities and differences in the resulting stratospheric sulfate aerosol distributions, alongside in the resulting atmospheric and surface climate responses. Similar simulations had previously only been performed with one climate model, CESM1(WACCM) (MacMartin et al., 2017). Our multi-model simulations therefore serve a dual purpose: i) to evaluate the responses to off-equatorial SO_2 injections in multiple climate models, understanding similarities and differences between different independent climate models, and, thus, to isolate sources of uncertainty in model SAI responses and identify future areas of improvements; and ii) to lay the basis for a future intercomparison between models using a feedback algorithm capable of achieving multiple temperature targets (MacMartin et al., 2017) similar to the one used in Tilmes et al. (2018a) to produce the Geoengineering Large Ensemble.

The simulated changes in stratospheric Aerosol Optical Depth were analyzed in terms of both their absolute magnitudes and the values normalized per unit of global mean AOD achieved. The latter assumes the the latitudinal distribution of simulated AOD remains similar under varying injection rates. Previous analyses of the GLENS results showed that this assumption holds, unless very large injections are considered that might noticeably modify the stratospheric circulation and prevent the aerosols from reaching the higher latitudes (Visioni et al., 2020). Our results in this work showed that in order to achieve similar global AOD values, the models considered would require different amount of Tg-SO_2/yr injected, with the largest differences for the model with a different, simpler, aerosol treatment (GISS-E2.1-G with bulk microphysics). By analyzing the results in terms of the normalized distributions, which bypasses the bias due to different simulated global mean AOD values under the same injection rate, the largest inter-model differences were found in the tropics (especially for the equatorial injections) and at very high latitudes, with models disagreeing on the amount of aerosols transported poleward.

Using a similar separation between the absolute magnitudes and the normalized latitudinal changes we analyzed the resulting surface temperature responses. As before, a large discrepancy between the two GISS versions and the other two models was identified for the global mean response, with the former showing a global cooling per unit AOD roughly a factor of two (for the bulk aerosol version) or three (for the modal aerosol version) times larger than that simulated by either CESM2-WACCM6 and UKESM1.0. When the surface temperature responses are normalized, however, models generally show a good agreement amongst them in terms of the overall latitudinal distribution of the temperature changes, and similarly they show a good agreement in the response of the latitudinal changes in precipitation.

Uncertainties in the projected SAI responses closely track those reported for simulations of past explosive volcanic eruptions (Clyne et al., 2021). Our results show that a large fraction of these uncertainties arise from discrepancies in the SO_2-to-sulfate aerosol conversion and their subsequent growth in the three models with three different model aerosol schemes, although differences in the stratospheric circulation also play an important role, as shown in PART2. In addition, comparison of the two sets of GISS simulations using either modal or bulk treatment of aerosol microphysics showed important differences in terms of

https://doi.org/10.5194/egusphere-2022-401
Preprint. Discussion started: 13 June 2022

the simulated AOD and the overall cooling produced per unit AOD (Figure 7), as well as in terms of the resulting stratospheric response (PART2), highlighting the importance of detailed treatment of microphysical processes. In agreement, a recent study from Laakso et al. (2022) using ECHAM-HAMMOZ showed that the choice of aerosol scheme (modal versus sectional) can lead to large discrepancies in the resulting radiative forcing due to the injection of different quantities of SO_2 (up to twice as large for some scenarios). Our GISS results here further confirm that the choice of aerosol microphysical scheme, all else being equal, can influence the overall amount of cooling, although the results are still even more influenced by the choice of climate model.

This work has shown that it would be feasible to replicate a global-scale injection strategy, such as the one used in GLENS, in multiple climate models; if the amount of SO_2 injected can be controlled year by year, models appear capable of reproducing a similar scaled surface temperature response. This thus ensures that a strategy including injections at 30°N, 15°N, 15°S and 30°S would potentially be able to maintain the three defined temperature targets (i.e. global mean surface temperature, and equator-to-pole and inter-hemispheric surface temperature gradients), albeit with differences in the injection magnitudes between models. A future comparison of the results of such an experiment using different climate models maintaining similar temperature targets would help identify different sources of uncertainty in the modelled response to SAI as compared to fixed-point injection simulations, for instance regarding the behavior of the Atlantic Meridional Overturning Circulation (Tilmes et al., 2020), the North Atlantic Oscillation (Jones et al., 2022) or impacts on middle atmospheric composition, including stratospheric ozone (Tilmes et al., 2021). When it comes to climate impacts, focusing on particular large-scale temperature targets rather analysing the direct outcomes of fixed single-point injections shifts, in a way, the focus from one kind of uncertainty to another. If the location and amount of injections can be modified, some of the stratospheric uncertainties discussed here would matter less, as the strategy could be adjusted to obtain a pattern of aerosol distribution functional to obtaining a certain pattern of cooling. The consistency in the normalized temperature response between models indeed seem to suggest this is possible. If similar large-scale patterns of cooling can be achieved consistently between models, more focus can then be given to understanding the uncertainties in the projected regional scale responses, which are an essential to properly assess local risks and adaptation strategies. This does not remove uncertainties related to the large scale transport of the aerosols, which are still important to resolve, but rather suggests they can be, in this way, studied separately (like it is done in detail in PART2 using these same simulations).

Code availability. The code used to calculate the matrices and figures in Section 5 is available at https://github.com/dan-visioni/code-for-gains-calculator.

Data availability. The data used in this work will be available in the Cornell eCommons repository upon publication of the preprint, and the link will be added upon publication. Please contact DV to access the data before that.

https://doi.org/10.5194/egusphere-2022-401
Preprint. Discussion started: 13 June 2022

Author contributions. DV performed the CESM2 simulations, wrote the manuscript and performed the analyses. EB performed the analyses and contributed to the manuscript. WRL performed the analyses and wrote the public code for Section 5 with help from DGM. AJ and JH performed the UKESM simulations. BK performed the GISS simulations. DGM contributed to the manuscript.

Competing interests. The authors declare no competing interests

Acknowledgements. Support was provided by the Atkinson Center for a Sustainable Future at Cornell University for DV, EMB and DGM. Support for B.K. was provided in part by the National Science Foundation through agreement CBET-1931641, the Indiana University Environmental Resilience Institute, and the *Prepared for Environmental Change* Grand Challenge initiative. The Pacific Northwest National Laboratory is operated for the US Department of Energy by Battelle Memorial Institute under contract DE-AC05-76RL01830. AJ and JMH were supported by the Met Office Hadley Centre Climate Programme funded by BEIS and by SilverLining through its Safe Climate Research Initiative.

The Community Earth System Model (CESM) project is supported primarily by the National Science Foundation. We would like to acknowledge high-performance computing support from Cheyenne (https://doi.org/10.5065/ D6RX99HX) provided by NCAR's Computational and Information Systems Laboratory, sponsored by the National Science Foundation. The UKESM simulations were carried out using MONSooN2, a collaborative High-Performance Computing facility funded by the Met Office and the Natural Environment Research Council. NASA GISS ModelE simulations were supported by the NASA High-End Computing (HEC) Program through the NASA Center for Climate Simulation (NCCS) at Goddard Space Flight Center. Data storage at Indiana University is supported by the National Science Foundation under Grant No. CNS-0521433.

https://doi.org/10.5194/egusphere-2022-401
Preprint. Discussion started: 13 June 2022

References

Archibald, A. T., O'Connor, F. M., Abraham, N. L., Archer-Nicholls, S., Chipperfield, M. P., Dalvi, M., Folberth, G. A., Dennison, F., Dhomse, S. S., Griffiths, P. T., Hardacre, C., Hewitt, A. J., Hill, R. S., Johnson, C. E., Keeble, J., Köhler, M. O., Morgenstern, O., Mulcahy, J. P., Ordóñez, C., Pope, R. J., Rumbold, S. T., Russo, M. R., Savage, N. H., Sellar, A., Stringer, M., Turnock, S. T., Wild, O., and Zeng, G.: Description and evaluation of the UKCA stratosphere–troposphere chemistry scheme (StratTrop vn 1.0) implemented in UKESM1, Geoscientific Model Development, 13, 1223–1266, 2020.

Banerjee, A., Butler, A. H., Polvani, L. M., Robock, A., Simpson, I. R., and Sun, L.: Robust winter warming over Eurasia under stratospheric sulfate geoengineering – the role of stratospheric dynamics, Atmospheric Chemistry and Physics Discussions, 2020, 1–20, https://doi.org/10.5194/acp-2020-965, 2020.

Bauer, S. E., Wright, D. L., Koch, D., Lewis, E. R., McGraw, R., Chang, L.-S., Schwartz, S. E., and Ruedy, R.: MATRIX (Multiconfiguration Aerosol TRacker of mIXing state): an aerosol microphysical module for global atmospheric models, Atmospheric Chemistry and Physics, 8, 6003–6035, 2008.

Bauer, S. E., Tsigaridis, K., Faluvegi, G., Kelley, M., Lo, K. K., Miller, R. L., Nazarenko, L., Schmidt, G. A., and Wu, J.: Historical (1850–2014) Aerosol Evolution and Role on Climate Forcing Using the GISS ModelE2.1 Contribution to CMIP6, Journal of Advances in Modeling Earth Systems, 12, e2019MS001 978, https://doi.org/https://doi.org/10.1029/2019MS001978, e2019MS001978 2019MS001978, 2020.

Boucher, O., Randall, D., Artaxo, P., Bretherton, C., Feingold, G., Forster, P., Kerminen, V.-M., Kondo, Y., Liao, H., Lohmann, U., Rasch, P., Satheesh, S., Sherwood, S., Stevens, B., and Zhang, X.: : Climate Change 2013: The Physical Science Basis. Contribution of Working Group I to the Fifth Assessment Report of the Intergovernmental Panel on Climate Change, in: Fifth Assessment Report of the Intergovernmental Panel on Climate Change, edited by IPCC, IPCC, https://www.ipcc.ch/site/assets/uploads/2018/02/WG1AR5_Chapter07_FINAL-1.pdf, 2013.

Brunner, L., Pendergrass, A. G., Lehner, F., Merrifield, A. L., Lorenz, R., and Knutti, R.: Reduced global warming from CMIP6 projections when weighting models by performance and independence, Earth System Dynamics, 11, 995–1012, 2020.

Clyne, M., Lamarque, J.-F., Mills, M. J., Khodri, M., Ball, W., Bekki, S., Dhomse, S. S., Lebas, N., Mann, G., Marshall, L., Niemeier, U., Poulain, V., Robock, A., Rozanov, E., Schmidt, A., Stenke, A., Sukhodolov, T., Timmreck, C., Toohey, M., Tummon, F., Zanchettin, D., Zhu, Y., and Toon, O. B.: Model physics and chemistry causing intermodel disagreement within the VolMIP-Tambora Interactive Stratospheric Aerosol ensemble, Atmospheric Chemistry and Physics, 21, 3317–3343, https://doi.org/10.5194/acp-21-3317-2021, 2021.

Crutzen, P. J.: Albedo Enhancement by Stratospheric Sulfur Injections: A Contribution to Resolve a Policy Dilemma?, Climatic Change, 77, 211–220, https://doi.org/10.1007/s10584-006-9101-y, 2006.

Danabasoglu, G., Lamarque, J.-F., Bacmeister, J., Bailey, D. A., DuVivier, A. K., Edwards, J., Emmons, L. K., Fasullo, J., Garcia, R., Gettelman, A., Hannay, C., Holland, M. M., Large, W. G., Lauritzen, P. H., Lawrence, D. M., Lenaerts, J. T. M., Lindsay, K., Lipscomb, W. H., Mills, M. J., Neale, R., Oleson, K. W., Otto-Bliesner, B., Phillips, A. S., Sacks, W., Tilmes, S., van Kampenhout, L., Vertenstein, M., Bertini, A., Dennis, J., Deser, C., Fischer, C., Fox-Kemper, B., Kay, J. E., Kinnison, D., Kushner, P. J., Larson, V. E., Long, M. C., Mickelson, S., Moore, J. K., Nienhouse, E., Polvani, L., Rasch, P. J., and Strand, W. G.: The Community Earth System Model Version 2 (CESM2), Journal of Advances in Modeling Earth Systems, 12, e2019MS001 916, https://doi.org/10.1029/2019MS001916, e2019MS001916 2019MS001916, 2020.

https://doi.org/10.5194/egusphere-2022-401
Preprint. Discussion started: 13 June 2022

Deser, C., Phillips, A., Bourdette, V., and Teng, H.: Uncertainty in climate change projections: the role of internal variability, Climate Dynamics, 38, 527–546, 2012.

Dhomse, S. S., Kinnison, D., Chipperfield, M. P., Salawitch, R. J., Cionni, I., Hegglin, M. I., Abraham, N. L., Akiyoshi, H., Archibald, A. T., Bednarz, E. M., Bekki, S., Braesicke, P., Butchart, N., Dameris, M., Deushi, M., Frith, S., Hardiman, S. C., Hassler, B., Horowitz, L. W., Hu, R. M., Jockel, P., Josse, B., Kirner, O., Kremser, S., Langematz, U., Lewis, J., Marchand, M., Lin, M., Mancini, E., Marecal, V., Michou, M., Morgenstern, O., O'Connor, F. M., Oman, L., Pitari, G., Plummer, D. A., Pyle, J. A., Revell, L. E., Rozanov, E., Schofield, R., Stenke, A., Stone, K., Sudo, K., Tilmes, S., Visioni, D., Yamashita, Y., and Zeng, G.: Estimates of ozone return dates from Chemistry-Climate Model Initiative simulations, Atmospheric Chemistry and Physics, 18, 8409–8438, https://doi.org/10.5194/acp-18-8409-2018, 2018.

Dhomse, S. S., Mann, G. W., Antuña Marrero, J. C., Shallcross, S. E., Chipperfield, M. P., Carslaw, K. S., Marshall, L., Abraham, N. L., and Johnson, C. E.: Evaluating the simulated radiative forcings, aerosol properties, and stratospheric warmings from the 1963 Mt Agung, 1982 El Chichón, and 1991 Mt Pinatubo volcanic aerosol clouds, Atmospheric Chemistry and Physics, 20, 13 627–13 654, https://doi.org/10.5194/acp-20-13627-2020, 2020.

Eichinger, R., Dietmuller, S., Garny, H., Sacha, P., Birner, T., Bonisch, H., Pitari, G., Visioni, D., Stenke, A., Rozanov, E., Revell, L., Plummer, D. A., Jockel, P., Oman, L., Deushi, M., Kinnison, D. E., Garcia, R., Morgenstern, O., Zeng, G., Stone, K. A., and Schofield, R.: The influence of mixing on the stratospheric age of air changes in the 21st century, Atmospheric Chemistry and Physics, 19, 921–940, 2019.

Gettelman, A., Mills, M. J., Kinnison, D. E., Garcia, R. R., Smith, A. K., Marsh, D. R., Tilmes, S., Vitt, F., Bardeen, C. G., McInerny, J., Liu, H.-L., Solomon, S. C., Polvani, L. M., Emmons, L. K., Lamarque, J.-F., Richter, J. H., Glanville, A. S., Bacmeister, J. T., Phillips, A. S., Neale, R. B., Simpson, I. R., DuVivier, A. K., Hodzic, A., and Randel, W. J.: The Whole Atmosphere Community Climate Model Version 6 (WACCM6), Journal of Geophysical Research: Atmospheres, 124, 12 380–12 403, https://doi.org/https://doi.org/10.1029/2019JD030943, 2019.

Hawkins, E. and Sutton, R.: The potential to narrow uncertainty in projections of regional precipitation change, Climate Dynamics, 37, 407–418, 2011.

Haywood, J. M., Jones, A., Bellouin, N., and Stephenson, D.: Asymmetric forcing from stratospheric aerosols impacts Sahelian rainfall, Nature Climate Change, 3, 660–665, 2013.

Jiang, J., Cao, L., MacMartin, D. G., Simpson, I. R., Kravitz, B., Cheng, W., Visioni, D., Tilmes, S., Richter, J. H., and Mills, M. J.: Stratospheric Sulfate Aerosol Geoengineering Could Alter the High-Latitude Seasonal Cycle, Geophysical Research Letters, 46, 14 153–14 163, https://doi.org/10.1029/2019GL085758, 2019.

Jones, A., Haywood, J. M., Jones, A. C., Tilmes, S., Kravitz, B., and Robock, A.: North Atlantic Oscillation response in GeoMIP experiments G6solar and G6sulfur: why detailed modelling is needed for understanding regional implications of solar radiation management, Atmospheric Chemistry and Physics, 21, 1287–1304, https://doi.org/10.5194/acp-21-1287-2021, 2021.

Jones, A., Haywood, J. M., Scaife, A. A., Boucher, O., Henry, M., Kravitz, B., Lurton, T., Nabat, P., Niemeier, U., Séférian, R., Tilmes, S., and Visioni, D.: The impact of stratospheric aerosol intervention on the North Atlantic and Quasi-Biennial Oscillations in the Geoengineering Model Intercomparison Project (GeoMIP) G6sulfur experiment, Atmospheric Chemistry and Physics, 22, 2999–3016, 2022.

Kelley, M., Schmidt, G. A., Nazarenko, L. S., Bauer, S. E., Ruedy, R., Russell, G. L., Ackerman, A. S., Aleinov, I., Bauer, M., Bleck, R., Canuto, V., Cesana, G., Cheng, Y., Clune, T. L., Cook, B. I., Cruz, C. A., Del Genio, A. D., Elsaesser, G. S., Faluvegi, G., Kiang, N. Y., Kim, D., Lacis, A. A., Leboissetier, A., LeGrande, A. N., Lo, K. K., Marshall, J., Matthews, E. E., McDermid, S., Mezuman, K., Miller,

https://doi.org/10.5194/egusphere-2022-401
Preprint. Discussion started: 13 June 2022

R. L., Murray, L. T., Oinas, V., Orbe, C., García-Pando, C. P., Perlwitz, J. P., Puma, M. J., Rind, D., Romanou, A., Shindell, D. T., Sun, S., Tausnev, N., Tsigaridis, K., Tselioudis, G., Weng, E., Wu, J., and Yao, M.-S.: GISS-E2.1: Configurations and Climatology, Journal of Advances in Modeling Earth Systems, 12, e2019MS002 025, https://doi.org/https://doi.org/10.1029/2019MS002025, e2019MS002025 10.1029/2019MS002025, 2020.

Koch, D., Schmidt, G. A., and Field, C. V.: Sulfur, sea salt, and radionuclide aerosols in GISS ModelE, Journal of Geophysical Research: Atmospheres, 111, https://doi.org/https://doi.org/10.1029/2004JD005550, 2006.

Kravitz, B., Robock, A., Boucher, O., Schmidt, H., Taylor, K. E., Stenchikov, G., and Schulz, M.: The Geoengineering Model Intercomparison Project (GeoMIP), Atmospheric Science Letters, 12, 162–167, https://doi.org/10.1002/asl.316, 2011.

Kravitz, B., Rasch, P. J., Forster, P. M., Andrews, T., Cole, J. N., Irvine, P. J., Ji, D., Kristjánsson, J. E., Moore, J. C., Muri, H., Niemeier, U., Robock, A., Singh, B., Tilmes, S., Watanabe, S., and Yoon, J. H.: An energetic perspective on hydrological cycle changes in the Geoengineering Model Intercomparison Project, Journal of Geophysical Research Atmospheres, 118, 13,087–13,102, https://doi.org/10.1002/2013JD020502, 2013.

Kravitz, B., Robock, A., Tilmes, S., Boucher, O., English, J. M., Irvine, P. J., Jones, A., Lawrence, M. G., MacCracken, M., Muri, H., Moore, J. C., Niemeier, U., Phipps, S. J., Sillmann, J., Storelvmo, T., Wang, H., and Watanabe, S.: The Geoengineering Model Intercomparison Project Phase 6 (GeoMIP6): simulation design and preliminary results, Geoscientific Model Development, 8, 3379–3392, https://doi.org/10.5194/gmd-8-3379-2015, 2015.

Kravitz, B., MacMartin, D. G., Wang, H., and Rasch, P. J.: Geoengineering as a design problem, Earth System Dynamics, 7, 469–497, https://doi.org/10.5194/esd-7-469-2016, 2016.

Kravitz, B., Lamarque, J.-F., Tribbia, J. J., Tilmes, S., Vitt, F., Richter, J. H., MacMartin, D. G., and Mills, M. J.: First Simulations of Designing Stratospheric Sulfate Aerosol Geoengineering to Meet Multiple Simultaneous Climate Objectives, Journal of Geophysical Research: Atmospheres, 122, 12,616–12,634, https://doi.org/10.1002/2017jd026874, 2017.

Kravitz, B., MacMartin, D. G., Tilmes, S., Richter, J. H., Mills, M. J., Cheng, W., Dagon, K., Glanville, A. S., Lamarque, J.-F., Simpson, I. R., Tribbia, J., and Vitt, F.: Comparing Surface and Stratospheric Impacts of Geoengineering With Different SO2 Injection Strategies, Journal of Geophysical Research: Atmospheres, 124, 7900–7918, https://doi.org/10.1029/2019JD030329, 2019.

Kuhlbrodt, T., Jones, C. G., Sellar, A., Storkey, D., Blockley, E., Stringer, M., Hill, R., Graham, T., Ridley, J., Blaker, A., Calvert, D., Copsey, D., Ellis, R., Hewitt, H., Hyder, P., Ineson, S., Mulcahy, J., Siahaan, A., and Walton, J.: The Low-Resolution Version of HadGEM3 GC3.1: Development and Evaluation for Global Climate, Journal of Advances in Modeling Earth Systems, 10, 2865–2888, https://doi.org/https://doi.org/10.1029/2018MS001370, 2018.

Laakso, A., Niemeier, U., Visioni, D., Tilmes, S., and Kokkola, H.: Dependency of the impacts of geoengineering on the stratospheric sulfur injection strategy – Part 1: Intercomparison of modal and sectional aerosol modules, Atmospheric Chemistry and Physics, 22, 93–118, 2022.

Lehner, F., Deser, C., Maher, N., Marotzke, J., Fischer, E. M., Brunner, L., Knutti, R., and Hawkins, E.: Partitioning climate projection uncertainty with multiple large ensembles and CMIP5/6, Earth System Dynamics, 11, 491–508, 2020.

Liu, X., Easter, R. C., Ghan, S. J., Zaveri, R., Rasch, P., Shi, X., Lamarque, J.-F., Gettelman, A., Morrison, H., Vitt, F., Conley, A., Park, S., Neale, R., Hannay, C., Ekman, A. M. L., Hess, P., Mahowald, N., Collins, W., Iacono, M. J., Bretherton, C. S., Flanner, M. G., and Mitchell, D.: Toward a minimal representation of aerosols in climate models: description and evaluation in the Community Atmosphere Model CAM5, Geoscientific Model Development, 5, 709–739, https://doi.org/10.5194/gmd-5-709-2012, 2012.

https://doi.org/10.5194/egusphere-2022-401
Preprint. Discussion started: 13 June 2022

Liu, X., Ma, P.-L., Wang, H., Tilmes, S., Singh, B., Easter, R. C., Ghan, S. J., and Rasch, P. J.: Description and evaluation of a new four-mode version of the Modal Aerosol Module (MAM4) within version 5.3 of the Community Atmosphere Model, Geoscientific Model Development, 9, 505–522, 2016.

MacMartin, D. G., Kravitz, B., Mills, M. J., Tribbia, J. J., Tilmes, S., Richter, J. H., Vitt, F., and Lamarque, J.-F.: The Climate Response to Stratospheric Aerosol Geoengineering Can Be Tailored Using Multiple Injection Locations, Journal of Geophysical Research: Atmospheres, 122, 12,574–12,590, https://doi.org/10.1002/2017jd026868, 2017.

Mann, G. W., Carslaw, K. S., Spracklen, D. V., Ridley, D. A., Manktelow, P. T., Chipperfield, M. P., Pickering, S. J., and Johnson, C. E.: Description and evaluation of GLOMAP-mode: a modal global aerosol microphysics model for the UKCA composition-climate model, Geoscientific Model Development, 3, 519–551, https://doi.org/https://doi.org/10.5194/gmd-13-6383-2020, 2010.

Masson, D. and Knutti, R.: Spatial-Scale Dependence of Climate Model Performance in the CMIP3 Ensemble, Journal of Climate, 24, 2680 – 2692, 2011.

McGraw, R.: Description of Aerosol Dynamics by the Quadrature Method of Moments, Aerosol Science and Technology, 27, 255–265, https://doi.org/10.1080/02786829708965471, 1997.

Meinshausen, M., Nicholls, Z. R. J., Lewis, J., Gidden, M. J., Vogel, E., Freund, M., Beyerle, U., Gessner, C., Nauels, A., Bauer, N., Canadell, J. G., Daniel, J. S., John, A., Krummel, P. B., Luderer, G., Meinshausen, N., Montzka, S. A., Rayner, P. J., Reimann, S., Smith, S. J., van den Berg, M., Velders, G. J. M., Vollmer, M. K., and Wang, R. H. J.: The shared socio-economic pathway (SSP) greenhouse gas concentrations and their extensions to 2500, Geoscientific Model Development, 13, 3571–3605, https://doi.org/10.5194/gmd-13-3571-2020, 2020.

Mills, M. J., Schmidt, A., Easter, R., Solomon, S., Kinnison, D. E., Ghan, S. J., Neely III, R. R., Marsh, D. R., Conley, A., Bardeen, C. G., and Gettelman, A.: Global volcanic aerosol properties derived from emissions, 1990–2014, using CESM1(WACCM), Journal of Geophysical Research: Atmospheres, 121, 2332–2348, https://doi.org/10.1002/2015JD024290, 2016.

Mills, M. J., Richter, J. H., Tilmes, S., Kravitz, B., Macmartin, D. G., Glanville, A. A., Tribbia, J. J., Lamarque, J. F., Vitt, F., Schmidt, A., Gettelman, A., Hannay, C., Bacmeister, J. T., and Kinnison, D. E.: Radiative and chemical response to interactive stratospheric sulfate aerosols in fully coupled CESM1(WACCM), Journal of Geophysical Research: Atmospheres, 122, 13,061–13,078, https://doi.org/10.1002/2017JD027006, 2017.

Morgenstern, O., Stone, K. A., Schofield, R., Akiyoshi, H., Yamashita, Y., Kinnison, D. E., Garcia, R. R., Sudo, K., Plummer, D. A., Scinocca, J., Oman, L. D., Manyin, M. E., Zeng, G., Rozanov, E., Stenke, A., Revell, L. E., Pitari, G., Mancini, E., Di Genova, G., Visioni, D., Dhomse, S. S., and Chipperfield, M. P.: Ozone sensitivity to varying greenhouse gases and ozone-depleting substances in CCMI-1 simulations, Atmospheric Chemistry and Physics, 18, 1091–1114, https://doi.org/10.5194/acp-18-1091-2018, 2018.

Mulcahy, J. P., Jones, C., Sellar, A., Johnson, B., Boutle, I. A., Jones, A., Andrews, T., Rumbold, S. T., Mollard, J., Bellouin, N., Johnson, C. E., Williams, K. D., Grosvenor, D. P., and McCoy, D. T.: Improved Aerosol Processes and Effective Radiative Forcing in HadGEM3 and UKESM1, Journal of Advances in Modeling Earth Systems, 10, 2786–2805, https://doi.org/https://doi.org/10.1029/2018MS001464, 2018.

Niemeier, U. and Timmreck, C.: What is the limit of climate engineering by stratospheric injection of SO2?, Atmospheric Chemistry and Physics, 15, 9129–9141, https://doi.org/10.5194/acp-15-9129-2015, 2015.

Oman, L., Robock, A., Stenchikov, G. L., and Thordarson, T.: High-latitude eruptions cast shadow over the African monsoon and the flow of the Nile, Geophysical Research Letters, 33, https://doi.org/https://doi.org/10.1029/2006GL027665, 2006.

https://doi.org/10.5194/egusphere-2022-401
Preprint. Discussion started: 13 June 2022

Richter, J. H., Tilmes, S., Mills, M. J., Tribbia, J. J., Kravitz, B., Macmartin, D. G., Vitt, F., and Lamarque, J. F.: Stratospheric dynamical response and ozone feedbacks in the presence of SO2 injections, Journal of Geophysical Research: Atmospheres, 122, 12,557–12,573, https://doi.org/10.1002/2017JD026912, 2017.

Schmidt, A., Mills, M. J., Ghan, S., Gregory, J. M., Allan, R. P., Andrews, T., Bardeen, C. G., Conley, A., Forster, P. M., Gettelman, A., Portmann, R. W., Solomon, S., and Toon, O. B.: Volcanic Radiative Forcing From 1979 to 2015, Journal of Geophysical Research: Atmospheres, 123, 12 491–12 508, https://doi.org/10.1029/2018JD028776, 2018.

Schmidt, G. A., Bader, D., Donner, L. J., Elsaesser, G. S., Golaz, J.-C., Hannay, C., Molod, A., Neale, R. B., and Saha, S.: Practice and philosophy of climate model tuning across six US modeling centers, Geoscientific Model Development, 10, 3207–3223, 2017.

Sellar, A. A., Jones, C. G., Mulcahy, J. P., Tang, Y., Yool, A., Wiltshire, A., O'Connor, F. M., Stringer, M., Hill, R., Palmieri, J., Woodward, S., de Mora, L., Kuhlbrodt, T., Rumbold, S. T., Kelley, D. I., Ellis, R., Johnson, C. E., Walton, J., Abraham, N. L., Andrews, M. B., Andrews, T., Archibald, A. T., Berthou, S., Burke, E., Blockley, E., Carslaw, K., Dalvi, M., Edwards, J., Folberth, G. A., Gedney, N., Griffiths, P. T., Harper, A. B., Hendry, M. A., Hewitt, A. J., Johnson, B., Jones, A., Jones, C. D., Keeble, J., Liddicoat, S., Morgenstern, O., Parker, R. J., Predoi, V., Robertson, E., Siahaan, A., Smith, R. S., Swaminathan, R., Woodhouse, M. T., Zeng, G., and Zerroukat, M.: UKESM1: Description and Evaluation of the U.K. Earth System Model, Journal of Advances in Modeling Earth Systems, 11, 4513–4558, https://doi.org/10.1029/2019MS001739, 2019.

Simpson, I., Tilmes, S., Richter, J., Kravitz, B., MacMartin, D., Mills, M., Fasullo, J., and Pendergrass, A.: The regional hydroclimate response to stratospheric sulfate geoengineering and the role of stratospheric heating, Journal of Geophysical Research: Atmospheres, 124, 2019JD031 093, https://doi.org/10.1029/2019JD031093, 2019.

Smith, W.: The cost of stratospheric aerosol injection through 2100, Environmental Research Letters, 15, 114 004, 2020.

Smyth, J. E., Russotto, R. D., and Storelvmo, T.: Thermodynamic and dynamic responses of the hydrological cycle to solar dimming, Atmospheric Chemistry and Physics, 17, 6439–6453, https://doi.org/10.5194/acp-17-6439-2017, 2017.

Tebaldi, C., Debeire, K., Eyring, V., Fischer, E., Fyfe, J., Friedlingstein, P., Knutti, R., Lowe, J., O'Neill, B., Sanderson, B., van Vuuren, D., Riahi, K., Meinshausen, M., Nicholls, Z., Tokarska, K. B., Hurtt, G., Kriegler, E., Lamarque, J.-F., Meehl, G., Moss, R., Bauer, S. E., Boucher, O., Brovkin, V., Byun, Y.-H., Dix, M., Gualdi, S., Guo, H., John, J. G., Kharin, S., Kim, Y., Koshiro, T., Ma, L., Olivié, D., Panickal, S., Qiao, F., Rong, X., Rosenbloom, N., Schupfner, M., Séférian, R., Sellar, A., Semmler, T., Shi, X., Song, Z., Steger, C., Stouffer, R., Swart, N., Tachiiri, K., Tang, Q., Tatebe, H., Voldoire, A., Volodin, E., Wyser, K., Xin, X., Yang, S., Yu, Y., and Ziehn, T.: Climate model projections from the Scenario Model Intercomparison Project (ScenarioMIP) of CMIP6, Earth System Dynamics, 12, 253–293, 2021.

Tilmes, S., Fasullo, J., Lamarque, J.-F., Marsh, D. R., Mills, M., Alterskjær, K., Muri, H., Kristjánsson, J. E., Boucher, O., Schulz, M., Cole, J. N. S., Curry, C. L., Jones, A., Haywood, J., Irvine, P. J., Ji, D., Moore, J. C., Karam, D. B., Kravitz, B., Rasch, P. J., Singh, B., Yoon, J.-H., Niemeier, U., Schmidt, H., Robock, A., Yang, S., and Watanabe, S.: The hydrological impact of geoengineering in the Geoengineering Model Intercomparison Project (GeoMIP), Journal of Geophysical Research: Atmospheres, 118, 11,036–11,058, https://doi.org/10.1002/jgrd.50868, 2013.

Tilmes, S., Richter, J. H., Mills, M. J., Kravitz, B., Macmartin, D. G., Vitt, F., Tribbia, J. J., and Lamarque, J. F.: Sensitivity of aerosol distribution and climate response to stratospheric SO2 injection locations, Journal of Geophysical Research: Atmospheres, 122, 12,591–12,615, https://doi.org/10.1002/2017JD026888, 2017.

https://doi.org/10.5194/egusphere-2022-401
Preprint. Discussion started: 13 June 2022

Tilmes, S., Richter, J. H., Kravitz, B., Macmartin, D. G., Mills, M. J., Simpson, I. R., Glanville, A. S., Fasullo, J. T., Phillips, A. S., Lamarque, J. F., Tribbia, J., Edwards, J., Mickelson, S., and Ghosh, S.: CESM1(WACCM) stratospheric aerosol geoengineering large ensemble project, Bulletin of the American Meteorological Society, 99, 2361–2371, https://doi.org/10.1175/BAMS-D-17-0267.1, 2018a.

Tilmes, S., Richter, J. H., Mills, M. J., Kravitz, B., MacMartin, D. G., Garcia, R. R., Kinnison, D. E., Lamarque, J. F., Tribbia, J., and Vitt, F.: Effects of Different Stratospheric SO2 Injection Altitudes on Stratospheric Chemistry and Dynamics, Journal of Geophysical Research: Atmospheres, 123, 4654–4673, https://doi.org/10.1002/2017JD028146, 2018b.

Tilmes, S., MacMartin, D. G., Lenaerts, J. T. M., van Kampenhout, L., Muntjewerf, L., Xia, L., Harrison, C. S., Krumhardt, K. M., Mills, M. J., Kravitz, B., and Robock, A.: Reaching 1.5 and 2.0C global surface temperature targets using stratospheric aerosol geoengineering, Earth System Dynamics, 11, 579–601, https://doi.org/10.5194/esd-11-579-2020, 2020.

Tilmes, S., Visioni, D., Jones, A., Haywood, J., Séférian, R., Nabat, P., Boucher, O., Bednarz, E. M., and Niemeier, U.: Stratospheric Ozone Response to Sulfate Aerosol and Solar Dimming Climate Interventions based on the G6 Geoengineering Model Intercomparison Project (GeoMIP) Simulations, Atmospheric Chemistry and Physics Discussions, 2021, 1–31, 2021.

Timmreck, C., Mann, G. W., Aquila, V., Hommel, R., Lee, L. A., Schmidt, A., Brühl, C., Carn, S., Chin, M., Dhomse, S. S., Diehl, T., English, J. M., Mills, M. J., Neely, R., Sheng, J., Toohey, M., and Weisenstein, D.: The Interactive Stratospheric Aerosol Model Intercomparison Project (ISA-MIP): motivation and experimental design, Geoscientific Model Development, 11, 2581–2608, https://doi.org/10.5194/gmd-11-2581-2018, 2018.

Trenberth, K. E. and Dai, A.: Effects of Mount Pinatubo volcanic eruption on the hydrological cycle as an analog of geoengineering, Geophysical Research Letters, 34, https://doi.org/https://doi.org/10.1029/2007GL030524, 2007.

Visioni, D., Pitari, G., Aquila, V., Tilmes, S., Cionni, I., Di Genova, G., and Mancini, E.: Sulfate geoengineering impact on methane transport and lifetime: results from the Geoengineering Model Intercomparison Project (GeoMIP), Atmospheric Chemistry and Physics, 17, 11 209–11 226, https://doi.org/10.5194/acp-17-11209-2017, 2017.

Visioni, D., MacMartin, D. G., Kravitz, B., Lee, W., Simpson, I. R., and Richter, J. H.: Reduced poleward transport due to stratospheric heating under stratospheric aerosols geoengineering, Geophysical Research Letters, 47, e2020GL089 470, https://doi.org/10.1029/2020GL089470, e2020GL089470 2020GL089470, 2020.

Visioni, D., MacMartin, D. G., Kravitz, B., Boucher, O., Jones, A., Lurton, T., Martine, M., Mills, M. J., Nabat, P., Niemeier, U., Séférian, R., and Tilmes, S.: Identifying the sources of uncertainty in climate model simulations of solar radiation modification with the G6sulfur and G6solar Geoengineering Model Intercomparison Project (GeoMIP) simulations, Atmospheric Chemistry and Physics, 21, 10 039–10 063, https://doi.org/10.5194/acp-21-10039-2021, 2021.

Visioni, D., Tilmes, S., Bardeen, C., Mills, M., MacMartin, D. G., Kravitz, B., and Richter, J. H.: Limitations of assuming internal mixing between different aerosol species: a case study with sulfate geoengineering simulations, Atmospheric Chemistry and Physics, 22, 1739–1756, 2022.

Walters, D., Baran, A. J., Boutle, I., Brooks, M., Earnshaw, P., Edwards, J., Furtado, K., Hill, P., Lock, A., Manners, J., Morcrette, C., Mulcahy, J., Sanchez, C., Smith, C., Stratton, R., Tennant, W., Tomassini, L., Van Weverberg, K., Vosper, S., Willett, M., Browse, J., Bushell, A., Carslaw, K., Dalvi, M., Essery, R., Gedney, N., Hardiman, S., Johnson, B., Johnson, C., Jones, A., Jones, C., Mann, G., Milton, S., Rumbold, H., Sellar, A., Ujiie, M., Whitall, M., Williams, K., and Zerroukat, M.: The Met Office Unified Model Global Atmosphere 7.0/7.1 and JULES Global Land 7.0 configurations, Geoscientific Model Development, 12, 1909–1963, 2019.

https://doi.org/10.5194/egusphere-2022-401
Preprint. Discussion started: 13 June 2022

690 Weisenstein, D. K., Visioni, D., Franke, H., Niemeier, U., Vattioni, S., Chiodo, G., Peter, T., and Keith, D. W.: A Model Intercomparison of Stratospheric Solar Geoengineering by Accumulation-Mode Sulfate Aerosols, Atmospheric Chemistry and Physics Discussions, 2021, 1–30, 2021.

Wiltshire, A. J., Burke, E. J., Chadburn, S. E., Jones, C. D., Cox, P. M., Davies-Barnard, T., Friedlingstein, P., Harper, A. B., Liddicoat, S., Sitch, S., and Zaehle, S.: JULES-CN: a coupled terrestrial carbon–nitrogen scheme (JULES vn5.1), Geoscientific Model Development, 695 14, 2161–2186, https://doi.org/10.5194/gmd-14-2161-2021, 2021.

Yool, A., Palmiéri, J., Jones, C. G., de Mora, L., Kuhlbrodt, T., Popova, E. E., Nurser, A. J. G., Hirschi, J., Blaker, A. T., Coward, A. C., Blockley, E. W., and Sellar, A. A.: Evaluating the physical and biogeochemical state of the global ocean component of UKESM1 in CMIP6 historical simulations, Geoscientific Model Development, 14, 3437–3472, https://doi.org/10.5194/gmd-14-3437-2021, 2021.

Zhang, Y., MacMartin, D. G., Visioni, D., and Kravitz, B.: How large is the design space for stratospheric aerosol geoengineering?, Earth 700 System Dynamics, 13, 201–217, 2022.